Gene silencing by double-stranded RNA from *C. elegans* neurons reveals functional mosaicism of RNA interference

Snusha Ravikumar, Sindhuja Devanapally, and Antony M Jose*

Department of Cell Biology and Molecular Genetics, University of Maryland, College Park, MD-20742.

*Corresponding author: Antony M Jose, Rm 2136, Bioscience Research Building (Bldg #413), University of Maryland, College Park, MD-20742. Phone no: 301-405-7028. E-mail: amjose@umd.edu

Keywords: RNA-dependent RNA polymerase; stochastic; systemic RNAi

GRAPHICAL ABSTRACT

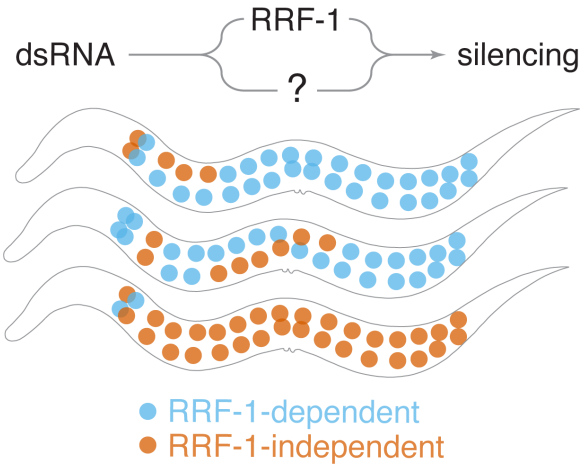

Double-stranded RNA (dsRNA) from neurons can bypass the requirement for the RNA-dependent RNA Polymerase RRF-1 to cause gene silencing in varying sets of intestinal cells.

ABSTRACT

Delivery of double-stranded RNA (dsRNA) into animals can silence genes of matching sequence in diverse cell types through mechanisms that have been collectively called RNA interference. In the nematode *C. elegans*, organism-wide silencing relies on the transport of dsRNA to cells and requires amplification of silencing signals. Amplification in somatic cells is thought to occur through the production of small RNAs by the RNA-dependent RNA Polymerase RRF-1. Here we show that the requirement for RRF-1 can vary based on the source of dsRNA, the target context, and even the particular cell examined. When the same intestinal target gene is silenced using ingested, intracellular, or neuronal dsRNA, only silencing by neuronal dsRNA is independent of RRF-1. When neuronal dsRNA is used to silence the same target sequence fused to different genes, the requirement for RRF-1 can differ. When both source and target are kept constant, different sets of intestinal cells show silencing in the absence of RRF-1 in different animals. Thus, the unequal and random availability of factor(s) that can compensate for the absence of RRF-1 in somatic cells suggests that each *C. elegans* animal is a functional mosaic with respect to RNA interference.

INTRODUCTION

Animals have diverse cell types that perform specialized functions while retaining the ability to perform common functions. Such common functions could rely on the same molecular machinery in all cells or on different machinery in different cells. As a result, an apparently uniform organismal response could obscure differences in the mechanisms used by different cells. A common response to viral infection is the silencing of viral genes facilitated by the recognition of viral double-stranded RNA (dsRNA) (reviewed in (1)). The experimental addition of dsRNA triggers similar mechanism(s) that can silence any matching sequence (2). This process of RNA interference is a powerful approach for gene silencing applications in a variety of organisms (reviewed in (3)). In the nematode *C. elegans*, exposure to multiple sources of dsRNA can silence matching genes in many somatic cell types and in the germline (1, 4-6). Studies in *C. elegans* have therefore been informative in piecing together the organismal response to RNAi in an animal. While similar silencing responses occur in diverse cell types, it is unclear whether dsRNA from every source engages the same molecular machinery in each cell.

Entry of extracellular dsRNA into the cytosol and subsequent silencing relies on the conserved dsRNA importer SID-1 (7-10). SID-1-dependent silencing is observed in many tissues even when dsRNA is expressed within a single tissue, suggesting that form(s) of dsRNA move between cells. In particular, dsRNA expressed in neurons can silence a target gene in somatic tissues such as the intestine, muscle, and hypodermis (11-13) and in the germline (14). Silencing in these diverse target cells requires the dsRNA-binding protein RDE-4 (15, 16) and the endonuclease DCR-1, which together processes dsRNA into small-interfering RNAs (siRNAs) (17, 18), and the Argonaute RDE-1, which binds siRNAs (19). Upon recognition of a matching mRNA by RDE-1-bound siRNAs, RNA-dependent RNA Polymerases (RdRPs) are recruited, resulting in the production of numerous secondary siRNAs (20, 21). Testing multiple target genes

suggests that two different RdRPs are used for silencing: RRF-1 for genes expressed in somatic cells (20-22) and EGO-1 for genes expressed in the germline (23, 24). Secondary siRNAs can bind the Argonaute NRDE-3 in somatic cells (25) or HRDE-1 in the germline (26-28) and subsequently accumulate within the nuclei of cells that express the target gene. Through these events, extracellular dsRNA can reduce the levels of mRNA and/or pre-mRNA of a target gene.

While silencing by all extracellular dsRNA requires SID-1, DCR-1, and RDE-1, the requirement for other components can vary. For example, some genes expressed in somatic cells can be silenced by ingested dsRNA in the absence of RRF-1 (29). While many genes do not require NRDE-3 for silencing, the *bli-1* gene requires NRDE-3 for silencing by ingested dsRNA or neuronal dsRNA (13). Finally, a strict requirement for NRDE-3 but not for RRF-1 is seen for the silencing of repetitive DNA that occurs in an enhanced RNAi background upon growth at lower temperatures (30). These observations suggest that a mix of mechanisms could underlie RNAi in *C. elegans.* Experiments that control one variable at a time are needed to elucidate features that dictate the choice of mechanism used for silencing.

Here we reveal that neuronal dsRNA differs from other sources of dsRNA in its requirement for RRF-1 to silence the same sequence and that changing genomic context of a target sequence can change the requirement for RRF-1. We provide a single-cell resolution view of silencing by neuronal dsRNA and find that each animal has a different complement of cells that require RRF-1 for gene silencing.

MATERIALS AND METHODS

Strains and Oligonucleotides Used: All strains (listed in Supplementary Table S1) were cultured on Nematode Growth Medium (NGM) plates seeded with 100 µl of OP50 at 20°C and mutant combinations were generated using standard methods (31). Sequences of oligonucleotides used to genotype different mutant combinations are in Supplementary Table S2 (*eri-1*: P01-P02, *mut-2/rde-3*: P03-P04, *mut-16*: P05-P06; *rde-1*: P07-P08, *rde-11*: P09-P10, *rrf-1*: P11-P13, and *sid-1*: P14-P15).

Transgenesis: *C. elegans* was transformed with plasmids and/or PCR products using microinjection (32) to generate extrachromosomal or integrated arrays. pHC337 was used to express an inverted repeat of *gfp* in neurons (11), which is expected to generate a hairpin RNA (*gfp-dsRNA*). Generation of the array that expresses *unc-22*-dsRNA in neurons (*qtEx136)* was described earlier (12). To rescue silencing defects in *rde-1(jam1)* and *rrf-1(jam3)* animals (Supplementary Figure S2), genomic DNA from wild-type animals (N2 gDNA) was used as a template to generate fused promoter/gene products through overlap extension PCR using Expand Long Template polymerase (Roche) and PCR products were purified using QIAquick PCR Purification Kit (Qiagen). The plasmid pHC448 for *DsRed2* expression in the pharynx or a PCR product, *Prgef-1::DsRed2::unc-54 3'UTR*, for *DsRed2* expression in neurons was used as a co-injection marker (12). Additional details are provided in Supplementary materials and methods.

Genome editing: Guide RNAs were transcribed in vitro and combined with Cas9 protein (PNA Bio Inc.) to generate complexes used for genome editing. To prepare guide RNAs, the scaffold DNA sequence was amplified from pDD162 (*Peft-3::Cas9* + Empty sgRNA - Addgene plasmid # 47549, a gift from Bob Goldstein) (33) using a common reverse primer

(P16) and target-specific forward primers (see Supplementary Table S2), purified (PCR Purification Kit, Qiagen), and used for in vitro transcription (SP6 RNA polymerase, NEB). Deletions were made using two guide RNAs and a single-stranded DNA oligonucleotide repair template with a co-conversion strategy (34). Insertions of *gfp* were performed using a single guide RNA and a double-stranded repair template amplified using PCR (35). *Punc-22::unc-22::gfp* resulted in GFP fluorescence within the pharynx as reported earlier (36).

Feeding RNAi: One generation of feeding RNAi was performed as described earlier (9) and the numbers of brightly fluorescent intestinal nuclei in animals subject to RNAi were counted.

Genetic screen and whole genome sequencing: AMJ1 animals were mutagenized with 25 mM N-ethyl N-nitrosourea (ENU, Toronto Research Chemicals) and ~600,000 of their F2 progeny were screened for recovery of GFP expression in intestinal cells (performed by A.M.J. in Craig Hunter's lab, Harvard University). We identified 23 mutants that showed different degrees of fluorescence and prepared genomic DNA from ~1-2 ml of worms for each mutant (200 - 800 ng/µl of DNA per mutant, NanoVue Plus (GE)). For each mutant, libraries for Illumina sequencing were prepared at the IBBR sequencing core as per manufacturer's instructions and sequenced using a HiSeq1000 (Illumina).

Bioinformatic Analysis: All bioinformatic analyses were done using the web-based Galaxy tool collection (https://usegalaxy.org) (37-39). For each of the 23 mutant strains, we obtained ~40 million 101 base fastq reads on average. One 5'-end base and three 3'-end bases were of lower quality and were trimmed from all reads before alignment to ce6/WS190 using Bowtie (~36 million mapped reads per mutant on average). Sequence

variants were filtered to call mutations (Phred33 ≥ 20, ≥ 2 aligned reads, and same variant call in ≥ 66% of reads). The threshold for calling a mutation was reduced from 66% to 15% for *sid-1* sequences to account for a non-functional copy with 12 missense mutations inadvertently included as part of *qtIs50* in all mutants (Supplementary Figure S1G). For all mutants, non-synonymous changes, changes in splice junctions, and deletions (characterized by lower than average coverage) were analyzed further. Identical changes detected in two or more mutants were eliminated as potential background mutations that were likely present before mutagenesis. Pairwise comparisons were carried out between all mutants to identify cases of different mutations in the same gene (i.e. in silico complementation (40), Supplementary Figure S1A). Because this process entails 253 pairwise comparisons, we expect that one or two such shared genes will be identified for some mutant pairs at random. For example, for mutant pairs with 30 mutated genes each, the p-value for one shared gene (0.044) and that for two shared genes (0.0009) are both larger than the Bonferroni corrected p-value of 0.0002 for 253 comparisons at $\alpha = 0.05$ (41).

Microscopy: For Figures 2A and 3B and Supplementary Figures S3B and S5B, animals were immobilized in 5µl of 3mM levamisole (Sigma-Aldrich; catalog no. 196142), mounted on slides, and imaged using an AZ100 microscope (Nikon) at a fixed magnification under non-saturating conditions of the tissue being quantified for silencing. A C-HGFI Intensilight Hg Illuminator was used to excite GFP (filter cube: 450-490 nm excitation, 495 nm dichroic, 500-550 nm emission), which also resulted in some bleed through from the DsRed fluorescence (e.g. Figure 3B). For Figure 4 and Supplementary Figure S7, L4-staged worms were mounted onto a slide with a 3.5% agarose pad after incubating the worm for 10 minutes in 7µl of 1mM freshly made levamisole. Extended exposure to levamisole was necessary for reliable immobilization of the worm for the ~100 minutes of imaging that was

required to obtain 512 x 512 images of entire L4-staged *sur-5::gfp* worms using a 63X lens in a Leica SP5X confocal microscope (average of 3 measurements per line, 319 slices per section, and 5 sections). A 488 nm laser was used to excite GFP (emission: 498-550nm, NA=1.4).

Image processing: All images being compared in a figure were adjusted identically using Photoshop (Adobe) and/or FIJI (NIH, (42)). Images taken on Nikon AZ100 were inverted (GFP = black), look-up tables were changed using Photoshop (190 = white and 255 = black for *gtbp-1::gfp*, *eft-3::gfp*, *gfp::unc-22* and *unc-22::gfp*; 212 = white and 255 = black for *sur-5::gfp*), and cropped for display. When imaging using the SP5X confocal (Figure 4 and Supplementary Figure S7), our immobilization conditions resulted in the worm lying on the coverslip such that the middle of the worm (vulva region) was tightly sandwiched between the coverslip and the agarose pad but the rest of the worm (head and tail in particular) was free to assume different positions. To partially account for this variability and the observed loss in sensitivity with depth of imaging, stacks close to the coverslip that lacked any signal were removed (0-30 stacks, median 7 stacks) and an equivalent number of empty stacks were added beyond the worm for a consistent total of 319 stacks in all cases. For Figure 4, Z-projections of the 5 stacks for each worm were stitched together using a combination of a pairwise stitching plugin (43) and manual alignment (Adobe Illustrator). For Figure 4A, each Z-stack was depth-coded using the 'temporal-color code' function in FIJI (6 colors with 53 stacks/color). For Supplementary Figure S7A, Z projections of maximum intensity were created using all 319 stacks (head and tail) or a subset of stacks (seam, uterus and vulva).

Quantification of silencing: Silencing in response to *unc-22*-dsRNA was scored by calculating the percentage of L4-staged animals that twitched within 3 min in 3mM

levamisole. The silencing of GFP expressed from *nrIs20* (*sur-5::gfp)* was determined by counting the number of intestinal nuclei that showed bright GFP fluorescence in L4-staged animals at a fixed magnification and zoom using a MVX10 stereomicroscope (Olympus). Average number of intestinal nuclei were determined by counting HC195 and was relatively constant in most genetic backgrounds with the exception of strains that lacked *rrf-1* (e.g. 32.8 ± 0.6 nuclei in *rrf-1(-); nrIs20* animals and 32.3 ± 0.8 nuclei in *rrf-1(-); eri-1(-) nrIs20* animals, compared to 29.9 ± 1.2 nuclei in *nrIs20* animals, errors indicate 95% CI). For images acquired using Nikon AZ100, silencing was quantified by measuring the fluorescence posterior to the pharynx in a region of interest (ROI) that included either a fixed area anterior to the germline (Figure 2 and Supplementary Figure S3) or body-wall muscles all along the worm (Figure 3 and Supplementary Figure S5), using the formula ROI fluorescence (arbitrary units) = intensity of ROI – (area of ROI X mean intensity of background). For images acquired using the SP5X confocal microscope, a combination of thresholding using the 3D object counter plugin (44) on FIJI (NIH) and manual verification was used to count various nuclei. To score nuclei as 'on' or 'off', different thresholds were used for intestinal nuclei located at different depths (70 for stacks 1-160; 20 for stacks 161-319) and a constant threshold was used for all other nuclei (20 for all stacks). The identity of each intestinal nucleus was inferred using its expected location and using the position of the vulva, anus, and the twisting rows of hypodermal cells (twist induced by the *rol-6* co-injection marker for *gfp*-dsRNA [qtIs49]) as guideposts (Figure 4F, (45-50)).

Statistics: Significance of differences in silencing (p-value < 0.05, unless otherwise stated) were calculated using Student's t-test (two tailed) or a two-way Analysis of Variation (ANOVA) with replication. Error bars in Figure 3D and Supplementary Figure S5D indicate 95% confidence intervals for single proportions calculated using Wilson's

estimates with a continuity correction (Method 4 in (51)) and significance of differences between strains was determined using pooled Wilson's estimates.

RESULTS

Silencing by neuronal dsRNA can be distinct from silencing by ingested or intracellular dsRNA

Double-stranded RNA can be introduced into *C. elegans* cells through the transcription of complementary sequences within the target cell, in a distant cell, or in ingested bacteria. While all these sources of dsRNA trigger RDE-1-dependent gene silencing (52), each source could produce different pools of dsRNA and/or dsRNA-derivatives that are trafficked differently to the cytosol of the target cell where silencing occurs. Here we present evidence that different sources of dsRNA can differ in their requirement for RRF-1 to silence the same target gene.

To examine silencing of a single target by different sources of dsRNA, we used a nuclear-localized GFP that is expressed in all somatic cells (*sur-5::gfp*) and is particularly prominent in the large intestinal nuclei (Figure 1A, *Top left*, ~30 GFP+ nuclei). This target is a multicopy transgene that generates trace amounts of intracellular dsRNA that can cause self-silencing in enhanced RNAi backgrounds (e.g. *adr-1(-); adr-2(-)* in (53) and *eri-1(-)* or *rrf-3(-)* in (30)). Silencing by this target-derived dsRNA was modest (Figure 1A, *Top right*, ~24 GFP+ nuclei in *eri-1(-)*, p-value < 10^{-3} when compared to ~30 GFP+ nuclei in *eri-1(+)*). Similarly, silencing by *gfp*-dsRNA expressed in neurons (*Prgef-1::gfp-dsRNA*) was also modest (Figure 1A, *Bottom left*, ~24 GFP+ nuclei, p-value < 10^{-4} when compared to *eri-1(+)*). However, when both target-derived and neuronal dsRNA were present together (i.e. in *eri-1(-); Prgef-1::gfp-dsRNA; sur-5::gfp* animals), we observed a synergistic effect resulting in greatly enhanced silencing (Figure 1A, *Bottom right*, ~3 GFP+ nuclei, two-way ANOVA p-value < 10^{-20} for interaction). These results are consistent with ERI-1 inhibiting both silencing by target-derived dsRNA (11, 30) and by neuronal dsRNA (12) (Figure 1B). Upon performing a genetic screen using these robustly silenced

animals, we isolated alleles of four genes with known roles in RNAi - *rde-1*, *rde-11*, *sid-1*, and *rrf-1* (Supplementary Figure S1). Surprisingly, unlike in null mutants of *rde-1* (Figure 1C), *rde-11* (Supplementary Figure S1E), or *sid-1* (Supplementary Figure S1F), significant silencing (p-value < 10^{-7}) was detectable in null mutants of *rrf-1* (Figure 1C) - a property shared by all three alleles of *rrf-1* isolated in the screen (Supplementary Figure S1C). Tissue-specific rescue experiments suggest that both *rde-1* and *rrf-1* function in the intestine (target cells) and not in neurons (source cells) to enable the observed silencing of intestinal cells (Supplementary Figure S2). Thus, when both target-derived dsRNA and neuronal dsRNA were used together to silence the same gene, RDE-1-dependent but RRF-1-independent silencing was detectable in some intestinal cells.

The observed RRF-1-independent silencing could be caused by target-derived dsRNA, neuronal dsRNA, or both. To determine the separate contribution of each source of dsRNA, we examined silencing by target-derived dsRNA using an *eri-1(-)* background and silencing by neuronal dsRNA in an *eri-1(+)* background. The weak silencing by target-derived dsRNA was completely abolished in *rrf-1* null mutants (Figure 1D *left*). Equally weak silencing by neuronal dsRNA was not significantly altered in *rrf-1* null mutants (Figure 1D *middle*). Yet, robust silencing by ingested dsRNA was strongly dependent on RRF-1 (Figure 1D *right*). These source-dependent differences in extents of silencing could be caused by differences in the routes taken by dsRNA to reach the silencing machinery, the forms of dsRNA, and/or the dosages of dsRNA. However, because weak silencing by neuronal dsRNA was independent of RRF-1 while strong silencing by ingested dsRNA was primarily dependent on RRF-1, a high dose of dsRNA from neurons cannot be the sole explanation for the observed RRF-1 independence. Therefore, these observations suggest that mechanisms engaged by ingested or target-derived dsRNA can differ from those engaged by neuronal dsRNA.

RRF-1-independent silencing can occur at multiple loci and relies on additional RNAi pathway components

To determine if silencing by neuronal dsRNA can occur in the absence of RRF-1 at other loci, we used the same source of neuronal dsRNA and examined silencing of GFP expression under the control of a different promoter introduced into different genomic loci. Silencing of *gfp* expressed under the control of the *eft-3* promoter (*Peft-3::gfp*) from a single-copy transgene was partially independent of RRF-1 (Figure 2A). In the absence of RRF-1, a significant reduction in GFP fluorescence was detectable (Figure 2B). A similar extent of RRF-1-independent silencing was observed using *Peft-3::gfp* transgenes located on three different chromosomes (Supplementary Figure S3A) and for a C-terminal *gfp* fusion of a ubiquitously expressed gene (Supplementary Figure S3B and Supplementary Figure S3C) generated using Cas9-based genome editing (Supplementary Figure S4A). Thus, a measurable amount of silencing by neuronal dsRNA can occur in the absence of RRF-1 when *gfp* is expressed under the control of different promoters and from different chromosomes.

Although it is formally possible that neuronal dsRNA engages novel processing pathways that are not used by other sources of dsRNA, we found that additional components of canonical RNAi were required for silencing (Figure 2B, *top*). RDE-11, thought to facilitate the production of secondary siRNA (54, 55), was required for most silencing (Figure 2B, *top*). MUT-16, a poly-Q/N protein (56) and MUT-2/RDE-3, a putative nucleotidyltransferase (57), that together localize to perinuclear foci thought to be sites of secondary siRNA production (58, 59), were both required for all observed silencing (Figure 2B, *top*). These results suggest that RRF-1-independent silencing by neuronal dsRNA either occurs through the action of primary siRNAs along with canonical factors such as RDE-11, MUT-16, and MUT-2/RDE-3, or through the production of secondary siRNAs using an alternative RdRP.

The *C. elegans* genome has four genes that encode proteins with RdRP domains, three of which have demonstrated roles in the production of RNA using RNA templates. RRF-3 is thought to act as a processive RdRP in an endogenous pathway (60, Supplementary Figure 9 in (61)) that competes with experimental RNAi for shared components (62) and therefore loss of *rrf-3* enhances RNAi (63). RRF-1 and EGO-1 are thought to act as non-processive RdRPs that make siRNAs in the soma (20, 21, 62) and the germline (64), respectively. Evaluation of their individual roles in experimental RNAi, however, is complicated by the sterility of *ego-1(-)* animals, reflecting the role of EGO-1 in the germline (23, 24). Preventing germline proliferation in *rrf-1(-)* animals was found to greatly reduce the levels of secondary siRNAs but not eliminate them (65), leaving open the possibility that the residual secondary siRNAs may be generated by an alternative RdRP. The fourth putative RdRP, RRF-2, was found to be not required for silencing by ingested dsRNA (22). To test if RRF-2 is responsible for the observed RRF-1-independent silencing by neuronal dsRNA, we generated a complete deletion of RRF-2 (Supplementary Figure S4B). Loss of *rrf-2* did not eliminate RRF-1-independent silencing but rather resulted in a modest enhancement of silencing (Figure 2B, *bottom*, two-way ANOVA p-value < 10^{-3} for interaction). Given these results, if secondary siRNAs are required for the RRF-1-independent silencing, remaining possibilities for their production could include an alternative role for RRF-3, somatic presence of EGO-1, or the use of an unknown RdRP.

Taken together, these results reveal instances of silencing in somatic cells by a source of neuronal dsRNA through a mechanism that is independent of the RdRP RRF-1 but that uses some canonical RNAi factors.

Context of target sequence can dictate the requirement for RRF-1

Expression of dsRNA in neurons does not always cause RRF-1-independent silencing. For example, neuronal dsRNA targeting *unc-22* ((12), Supplementary Figure S5A) or *bli-1* (Supplementary Figure S5A) required RRF-1 for any detectable silencing. Nevertheless, targeting *gfp* sequences using neuronal dsRNA resulted in RRF-1-independent silencing (in Figures 1 and 2, and Supplementary Figure S3 using an integrated *gfp*-dsRNA source, and in 6/6 *rrf-1(-); gtbp-1::gfp* animals using an extrachromosomal *gfp*-dsRNA source). These results suggest that RRF-1-independent silencing is not a generic property of all neuronal dsRNA and raise two possibilities: (1) sources that do not strictly require RRF-1 (e.g. neuronal *gfp*-dsRNA) differ from sources that require RRF-1 (e.g. neuronal *unc-22*-dsRNA); or (2) target sequences that do not strictly require RRF-1 (e.g. *gfp*) differ from target sequences that require RRF-1 (e.g. *unc-22*).

To examine silencing of a single target sequence by either source of dsRNA, we generated two chimeric genes (*unc-22::gfp* or *gfp::unc-22*) that could both be silenced by either *unc-22*-dsRNA or *gfp*-dsRNA expressed in neurons. Both chimeric genes express *unc-22* and *gfp* sequences as a single RNA under the control of endogenous *unc-22* regulatory sequences (Supplementary Figure S4C) and were functional as evidenced by lack of twitching (Figure 3D), which is a sensitive readout of reduction in *unc-22* function (2). With either source of dsRNA, all measurable silencing required RRF-1 (Figure 3 and Supplementary Figure S5). This complete dependence on RRF-1 was more evident when twitching was measured in response to the expression of either *gfp*-dsRNA (Figure 3D) or *unc-22*-dsRNA (Supplementary Figure S5D) in neurons.

These results suggest that changing the context of a sequence can change its dependence on RRF-1 for silencing by neuronal dsRNA. The attribute(s) of the context that determine whether RRF-1 is required for silencing could include genomic location, associated regulatory elements, or site of expression.

Cells that show RRF-1-independent silencing vary from animal to animal

To examine dependence on RRF-1 for silencing in all somatic cells while keeping the genomic location and associated regulatory elements of the target gene constant, we generated a chimeric gene with *gfp* sequence fused to the endogenous *sur-5* gene (*sur-5::gfp,* Supplementary Figure S4D). This strain resulted in the expression of a nuclear-localized SUR-5::GFP fusion protein, enabling simultaneous visualization of every somatic nucleus using confocal microscopy (Figure 4A). Expression of *gfp*-dsRNA in neurons resulted in silencing throughout the length of the animal that was entirely dependent on SID-1, consistent with silencing by neuronal dsRNA (Figure 4B and Figure 4C) and was not subject to silencing upon *eri-1* loss by target-derived dsRNA (Supplementary Figure S6A-C) as is expected for a single-copy target (30). Silencing was easily detected in intestinal cells, hypodermal cells, body-wall muscle cells, and the excretory canal cell (Figure 4B and Supplementary Figure S7A). Silencing was not detectable in some cells in the head region, the vulval and uterine regions, and occasionally in the tail region (Supplementary Figure S7A). Interestingly, even neighboring, lineal sister cells sometimes showed very different extents of silencing (e.g., intestinal cells near the tail in Supplementary Figure S7A). Nevertheless, the overall silencing observed was much more than that observed when the same source of dsRNA was used to silence a multi-copy *sur-5::gfp* transgene (1.0±0.4 visible intestinal nuclei for single-copy *sur-5::gfp* (Supplementary Figure S6C) versus 24.0±1.9 visible intestinal nuclei for multi-copy *sur-5::gfp* (Figure 1A), p-value < 10^{-21} and errors indicate 95% CI). A simple explanation for this difference could be that silencing higher numbers of target transcripts requires higher amounts of dsRNA (see Discussion for additional possibilities). Thus, the single-copy *sur-*

5::gfp gene is a sensitive target for evaluating RRF-1-independent silencing by neuronal dsRNA in cells throughout the animal.

Silencing of *sur-5::gfp* by neuronal dsRNA was detectable in *rrf-1(-)* animals (Figure 4D), but the extent of silencing and the locations of cells that showed silencing varied dramatically from animal to animal (Supplementary Figure S6D). To obtain a high-resolution view of silencing, we quantified silencing in multiple tissues by counting the number of nuclei that show fluorescence. For quantifying silencing in hypodermal and body-wall muscle cells, we divided the body into three regions: head (anterior to the posterior bulb of the pharynx), anterior body (anterior to the vulva), and posterior body (posterior to the vulva). In the head and anterior body, the average numbers of detectable nuclei in *rrf-1(-)* animals were not very different from the average numbers detectable in *sid-1(-)* animals (Supplementary Figure S7B). The posterior body, however, showed marginal silencing of hypodermal and/or body-wall muscle cells in *rrf-1(-)* animals (50.0±7.6 nuclei versus 58.7±4.6 nuclei in *sid-1(-)*, p-value = 0.08 and errors indicate 95%CI), suggestive of some RRF-1-independent silencing. The intestine, however, showed obvious RRF-1-independent silencing (Figure 4E). Because each of the 20 intestinal cells has an invariable lineal origin and position after morphogenesis (Figure 4F, (45-50)), we were able to examine whether silencing occurs in any discernable patterns correlated with lineage or position. Each tested worm had a different complement of cells that showed RRF-1-independent silencing (Figure 4F and Supplementary Figure S6D) and no cell was either RRF-1-dependent or RRF-1-independent in every animal (Figure 4F).

Together, these results show that neuronal dsRNA can cause robust silencing, but the particular cells that require RRF-1 for such silencing vary from animal to animal.

DISCUSSION

We examined RNA interference in the somatic cells of *C. elegans* and found that the source of extracellular dsRNA, the context of target sequences, and the identity of the tested cell can all dictate whether the RNA-dependent RNA polymerase RRF-1 is required for silencing. We discovered that silencing by neuronal dsRNA can be extensive and, when examined at single-cell resolution, different sets of cells showed RRF-1-independent silencing in each animal.

Silencing by neuronal dsRNA

Expression of dsRNA in all neuronal cells resulted in SID-1-dependent silencing in a variety of cell types throughout the animal (hypodermal cells, body-wall muscle cells, seam cells, intestinal cells, and excretory canal cell; Figure 4 and Supplementary Figure S7), suggesting that dsRNA molecules exported from neurons are widely available. Subsequent import depends on the levels of SID-1 in importing cells because cells that overexpress SID-1 can act as sinks for dsRNA and presumably reduce entry of dsRNA into other cells (Supplementary Figure S2 in (11), (66)). The observed widespread silencing (Figure 4) therefore suggests that no single tissue acts as a sink and that sufficient dsRNA is exported from neurons for entry into most cells.

Cells in some tissues (pharynx, vulva, and uterus), however, did not show appreciable silencing (Supplementary Figure S7A), reflecting inability of dsRNA to reach these specific tissues, inefficient import of dsRNA into cells in these tissues, or inefficient silencing. Similarly, silencing was observed only in a few random intestinal cells when the same source of neuronal dsRNA was used to silence a multi-copy *sur-5::gfp* transgene (Figure 1A). However, silencing was greatly enhanced upon loss of *eri-1* (Figure 1A), which releases shared factors used for endogenous RNAi-related processes (67). Therefore, this case of limited silencing by neuronal dsRNA likely reflects limited

availability of such RNAi factors (e.g. RDE-4, DCR-1, etc.) and not poor access to dsRNA or poor import of dsRNA.

Silencing in somatic cells in the absence of the RdRP RRF-1

Early RNAi studies proposed that amplification of silencing signals by RRF-1 is required for silencing somatic target genes in intact worms (22) and in extracts (68). Yet, we observed RRF-1-independent silencing by neuronal dsRNA (Figure 1, 2, 4, and Supplementary Figure S3 and S6) and similar RRF-1-independent silencing was reported using different ingested dsRNA sequences to target different genes (29). Using a single source of neuronal dsRNA to target the same sequence (*gfp*) in different contexts (*Peft-3::gfp* [x4 chromosomal locations], *Pgtbp-1::gtbp-1::gfp*, *Punc-22::gfp::unc-22*, *Punc-22::unc-22::gfp*, and *Psur-5::sur-5::gfp*), we avoid differences in dsRNA source or target sequence and establish that silencing in intestinal cells can be RRF-1-independent. This RRF-1-independent silencing, nevertheless, required MUT-16 (Figure 2) – a nucleator of secondary small RNA production sites (58, 59). Secondary small RNAs could be made at such sites by another RdRP that is selectively active in intestinal cells – our results exclude RRF-2 (Figure 2B) but somatic presence of the germline RdRP EGO-1 or a cryptic RdRP remain as possibilities. Alternatively, primary small RNAs could be sufficient for the observed RRF-1-independent silencing, but the failure to observe any silencing using an excess of primary siRNAs in *rrf-1(-)* animals (22) could argue against this possibility. Finally, evolutionary comparisons of mechanisms that control transposons in other nematodes and in arthropods point to other ways of achieving efficient silencing in the absence of RRF-1-like RdRPs (e.g. using RRF-3-like processive RdRPs (60) or without any RdRPs (60, 69)). Distinguishing between these possibilities requires additional experiments that dissect the mechanistic basis of RRF-1-independent silencing.

Functional mosaicism of RNAi in an animal

The identities of the intestinal cells that show RRF-1-independent silencing by neuronal dsRNA varied from animal to animal (Figure 4F and Supplementary Figure S6). This variation observed in *rrf-1(-)* animals reveals the unequal and random availability of factor(s) that can compensate for the absence of RRF-1. Such functional mosaicism is masked in wild-type animals, where the amplification of silencing signals by RRF-1 dampens variation. Thus, RRF-1 promotes silencing by extracellular dsRNA to ensure uniform silencing - a role that is reminiscent of the role for ERI-1 in opposing silencing by transgene-derived dsRNA to ensure uniform expression (30).

RNAi is an antiviral mechanism in many organisms (see (70) for the latest evolutionary perspective) and wild strains that are defective in RNAi can harbor viruses (71). Viral infection of *C. elegans* in the lab results in proliferation of the virus in some but not all intestinal cells (72). It would be interesting to determine whether mosaicism of specific components of the RNAi machinery underlies patterns of viral infection observed in the intestine of *Caenorhabditis* nematodes (71, 72). Analyses of variation in intact animals where organismal regulatory mechanisms are preserved, as described here using *C. elegans,* are an effective complement to analyses in single cells, which have begun to reveal heterogeneity in many processes (e.g. in gene expression (73), in membrane trafficking (74), and in subcellular organization (75)). We speculate that functional mosaicism and its control could be common in multicellular organisms because of the need to balance diversification of cell types with preservation of fundamental functions in all cells.

DATA AVAILABILITY

All strains and original confocal images are available upon request. Whole genome sequencing data for *rrf-1(jam2, jam3* and *jam4), rde-1(jam1), rde-11(jam50* and *jam51)* and *sid-1(jam52)* are available on Sequence Read Archive (PRJNA486008).

ACKNOWLEDGEMENTS

We thank Leslie Pick and members of the Jose lab for critical comments on the manuscript; Amy Beaven at the University of Maryland's imaging core for microscopy advice, Suwei Zhao at the IBBR sequencing facility for whole genome sequencing of mutants, Molly Lutrey for complementation analysis of *rde-11* mutants, Pravrutha Raman for preparation of genomic DNA from two mutants, the *Caenorhabditis elegans* Genetic stock Center, the Hunter lab (Harvard University), the Seydoux lab (Johns Hopkins University) and the Jorgensen lab (University of Utah) for some worm strains, and the Hamza lab (University of Maryland) for bacteria that express *gfp*-dsRNA.

FUNDING

This work was supported by a National Institutes of Health Grant [R01GM111457 to A.M.J.]. Funding for open access charge: National Institutes of Health.

CONFLICT OF INTEREST

The authors declare no conflict of interest.

REFERENCES

1. Obbard, D.J., Gordon, K.H., Buck, A.H. and Jiggins, F.M. (2009) The evolution of RNAi as a defence against viruses and transposable elements. *Philos Trans R Soc Lond B Biol Sci.*, **364**, 99-115.

2. Fire, A., Xu, S., Montgomery, M.K., Kostas,S.A., Driver, S.E. and Mello, C.C. (1998) Potent and specific genetic interference by double-stranded RNA in *Caenorhabditis elegans*, *Nature*, **391**, 806-11.

3. Perrimon, N., Ni, J.Q. and Perkins, L. (2010) In vivo RNAi: today and tomorrow. *Cold Spring Harb Perspect Biol.*, **2**, a003640.

4. Timmons,L. and Fire,A. (1998) Specific interference by ingested dsRNA. *Nature*, **395**, 854.

5. Tabara, H., Grishok, A. and Mello, C.C. (1998) RNAi in *C. elegans*: soaking in the genome sequence. *Science*, **282**, 430-1.

6. Tavernerakis, N., Wang, S.L., Dorovkov, M., Ryazanov, A. and Driscoll, M. (2000) Heritable and inducible genetic interference by double-stranded RNA encoded by transgenes. *Nat Genet*, **24**, 180-3.

7. Winston,W.M., Molodowitch,C. and Hunter,C.P. (2002) Systemic RNAi in *C. elegans* requires the putative transmembrane protein SID-1. *Science*, **295**, 2456-2459.

8. Feinberg,E.H. and Hunter,C.P. (2003) Transport of dsRNA into cells by the transmembrane protein SID-1. *Science*, **301**: 1545-1547.

9. Marré,J., Traver,E.C. and Jose,A.M. (2016) Extracellular RNA is transported from one generation to the next in *Caenorhabditis elegans*. *Proc Natl Acad Sci U S A.*, **113**,12496-12501.

10. Wang, E. and Hunter C.P. (2017) SID-1 Functions in Multiple Roles to Support Parental RNAi in *Caenorhabditis elegans*. *Genetics,* **207**, 547-557.

11. Jose, A.M., Smith,J.J. and Hunter,C.P. (2009) Export of RNA silencing from *C. elegans* tissues does not require the RNA channel SID-1. *Proc. Natl. Acad. Sci. U.S.A.*, **106**, 2283-2288.

12. Jose, A.M., Garcia,G.A. and Hunter,C.P. (2011) Two classes of silencing RNAs move between *C. elegans* tissues. *Nat. Struct. Mol. Biol.*, **18**, 1184-1188.

13. Raman,P., Zaghab, S.M., Traver, E.C. and Jose, A.M. (2017) The double-stranded RNA binding protein RDE-4 can act cell autonomously during feeding RNAi in *C. elegans*. *Nucleic Acids Res.,* **45**, 8463-8473.

14. Devanapally, S., Ravikumar, S. and Jose, A.M. (2015) Double-stranded RNA made in *C. elegans* neurons can enter the germline and cause transgenerational gene silencing. *Proc Natl Acad Sci U S A.* **112**,2133-8.

15. Tabara,H., Yigit,E., Siomi,H. and Mello,C.C. (2002) The dsRNA binding protein RDE-4 interacts with RDE-1, DCR-1, and a DExH-box helicase to direct RNAi in *C. elegans*. *Cell*, **109**, 861-71.

16. Parker,G.S., Eckert,D.M. and Bass,B.L. (2006) RDE-4 preferentially binds long dsRNA and its dimerization is necessary for cleavage of dsRNA to siRNA. *RNA*, **12**, 807-18.

17. Ketting, R.F., Fischer, S.E., Bernstein, E., Sijen, T., Hannon, G.J. and Plasterk, R.H. (2001) Dicer functions in RNA interference and in synthesis of small RNA involved in developmental timing in *C. elegans*. *Genes Dev*., **15**, 2654-9.

18. Knight, S.W. and Bass, B.L. (2001) A role for the RNase III enzyme DCR-1 in RNA interference and germ line development in *C. elegans*, *Science*, **293**, 2269-71.

19. Tabara,H., Sarikissian,M., Kelly, W.G., Fleenor,J., Grishok,A., Timmons,L., Fire,A. and Mello,C.C. (1999) The *rde-1* gene, RNA interference, and transposon silencing in *C. elegans*. *Cell*. **99**, 123-32.

20. Pak,J. and Fire,A. (2007) Distinct populations of primary and secondary effectors during RNAi in *C. elegans*. *Science*, **315**, 241-4.

21. Sijen,T., Steiner,F.A., Thijssen,K.L. and Plasterk,R.H. (2007) Secondary siRNAs result from unprimed RNA synthesis and form a distinct class. *Science*, **315**, 244-7.

22. Sijen,T., Fleenor,J., Simmer,F., Thijssen,K.L., Parrish,S., Timmons,L., Plasterk,R.H. and Fire,A. (2001) On the role of RNA amplification in dsRNA-triggered gene silencing. *Cell*. **107**, 465-76.

23. Smardon, A., Spoerke, J.M., Stacey, S.C., Klein, M.E., Mackin, N., Maine, E.M. (2000) EGO-1 is related to RNA-directed RNA Polymerase and functions in germ-line development and RNA interference in *C. elegans*. *Curr Biol.,* **10**, 167-78.

24. Vought, V.E., Ohmachi, M., Lee, M.H. and Maine, E.M. (2005). EGO-1 a putative RNA-directed RNA polymerase, promotes germline proliferation in parallel with GLP-1/notch signaling and regulates the spatial organization of nuclear pore complexes and germline P granules in *Caenorhabditis elegans*. *Genetics,* **10,** 169-78.

25. Guang,S., Bochner,A.F., Pavelec,D.M., Burkhart,K.B., Harding,S., Lachowiec,J. and Kennedy,S. (2008) An Argonaute transports siRNAs from the cytoplasm to the nucleus. *Science*, **321**, 537-541.

26. Ashe, A., Sapetschnig, A., Weick, E.M., Mitchell, J., Bagijn, M.P., Cording, A.C., Doebley, A.L., Goldstein, L.D., Lehrbach, N.J., Le Pen, J., *et al*. (2012) piRNAs can trigger a multigenerational epigenetic memory in the germline of *C. elegans*. *Cell*, **150**, 88-99.

27. Buckley, B.A., Burkhart, K.B., Gu, S.G., Spracklin, G., Kershner, A., Fritz, H., Kimble, J., Fire, A. and Kennedy, S. (2012) A nuclear Argonaute promotes multigenerational epigenetic inheritance and germline immortality. *Nature,* **489**, 447-51.

28. Shirayama, M., Seth, M., Lee, H.C., Gu, W., Ishidate, T., Conte, D. Jr. and Mello, C.C. (2012) piRNAs initiate an epigenetic memory of nonself RNA in the *C. elegans* germline. *Cell*, **150**, 65-77.

29. Kumsta, C. and Hansen, M. (2012) *C. elegans rrf-1* mutations maintain RNAi efficiency in the soma in addition to the germline. *PLoS One,* **7,** e35428.

30. Le,H.H., Looney,M., Strauss,B., Bloodgood,M. and Jose,A.M. (2016) Tissue homogeneity requires inhibition of unequal gene silencing during development. *J Cell Biol*., **214**, 319-31.

31. Brenner,S. (1974) The genetics of *Caenorhabditis elegans*. *Genetics*, **77**, 71-94.

32. Mello,C.C., Kramer,J.M., Stinchcomb,D. and Ambros,V. (1991) Efficient gene transfer in *C.elegans*: extrachromosomal maintenance and integration of transforming sequences. *EMBO J*. **10**, 3959-70.

33. Dickinson, D.J., Ward, J.D., Reiner, D.J. and Goldstein, B. (2013) Engineering the *Caenorhabditis elegans* genome using Cas9- triggered homologous recombination. *Nat Methods,* **10**, 1028-34.

34. Arribere,J.A., Bell,R.T., Fu,B.X., Artiles,K.L., Hartman,P.S. and Fire,A.Z. (2014) Efficient marker-free recovery of custom genetic modifications with CRISPR/Cas9 in *Caenorhabditis elegans*. *Genetics*, **198**, 837-846.

35. Paix, A., Wang, Y., Smith, H.E., Lee, C.Y., Calidas, D., Lu, T., Smith, J., Schmidt, H., Krause, M.W. and Seydoux, G. (2014) Scalable and versatile genome editing using linear DNAs with microhomology to Cas9 Sites in *Caenorhabditis elegans*. Genetics, **198**, 1347-56.

36. Matsunga, Y., Hwang, H., Franke, B., Williams, R., Penley, M., Qudota, H., Yi, H., Morran, L.T., Lu, H., Mayans, O. *et al.* (2017) Twitchin kinase inhibits muscle activity. *Mol Biol Cell*, **28**, 1591-1600.

37. Goecks, J., Nektrutenko, A., Taylor, J., Galaxy Team. (2010) Galaxy: a comprehensive approach for supporting accessible, reproducible, and transparent computational research in the life sciences. *Genome Biol.,* **11***,* R86.

38. Blankenberg, D., Von Kuster, G., Coraor, N., Ananda, G., Lazarus, R., Mangan, M., Nekrutenko, A. and Taylor, J. (2010) Galaxy: a web-based genome analysis tool for experimentalists. *Curr Proctoc Mol Biol.* **19**, 1-21.

39. Giardine, B., Riemer, C., Hardison, R.C., Burhans, R., Elnitski, L., Shah, P., Zhang, Y., Blankenberg, D., Albert, I., Taylor, J. *et al.* (2005) Galaxy: a platform for interactive large-scale genome analysis. *Genome Res.,* **15**, 1451-5.

40. Minevich, G., Park, D.S., Blankenberg, D, Poole, R.J. and Hobert, O. (2013) CloudMap: a cloud-based pipeline for analysis of mutant genome sequences. *Genetics*., **192**, 1249-69.

41. Miller, R.G., Jr. (1981) Simultaneous statistical inference. McGraw-Hill, New York, NY, USA.

42. Schindelin, J., Arganda-Carreras, I., Frise, E., Kaynig, V., Longair, M., Pietzsch, T., Preibisch, S., Rueden, C., Saalfeld, S., Schmid, B. *et al.* (2012) Fiji: an open- source platform for biological- image analysis. *Nat Methods*, **9**, 676-82.

43. Preibisch, S., Saalfeld, S. and Tomancak, P.. (2009) Globally optimal stitching of tiled 3D microscopic image acquisitions. *Bioinformatics*, **25**,1463–5.

44. Bolte, S. and Cordelières, F.P. (2006) A guided tour into subcellular colocalization analysis in light microscopy. *J Microsc*, **224**, 213-32.

45. Sulston, J. E. and Horvitz, H.R. (1977) Post-embryonic cell lineage of the nematode, *Caenorhabditis elegans*. *Dev. Biol.,* **56**, 110-156.

46. Sulston, J. E., Schierenberg, E., White, J.G, and Thompson, J.N. (1983) The embryonic cell lineage of the nematode *Caenorhabditis elegans. Dev. Biol.,* **100**, 64-119.

47. Leung, B., Hermann, G.J. and Priess, J.R. (1999) Organogenesis of the *Caenorhabditis elegans* intestine. *Dev. Biol.,* **216**, 114-134.

48. Hermann, G. J., Leung, B. and Priess, J.R. (2000) Left-right asymmetry in C. elegans intestine organogenesis involves a LIN-12/Notch signaling pathway. *Development,* **127**, 3429-3440.

49. Mendenhall, A. R., Tedesco, P.M., Sands, B., Johnson, T.E. and Brent, R. (2015) Single cell quantification of reporter gene expression in live adult *Caenorhabditis elegans* reveals reproducible cell-specific expression patterns and underlying biological variation. *PLoS One*, **10**, e0124289.

50. Asan, A., Raiders, S. A. and Priess, J. R. (2016) Morphogenesis of the *C. elegans* Intestine Involves Axon Guidance Genes. *PLoS Genet*. **12**, e1005950.

51. Newcombe, R.G. (1998) Two-sided confidence intervals for the single proportion: comparison of seven methods. *Statist. Med.*, **17**, 857-872.

52. Grishok, A.(2013) Biology and mechanisms of short RNAs in *Caenorhabditis elegans*. *Adv. Genetics*, **83**, 1-69.

53. Hellwig, S. and Bass,B.L. (2008) A starvation-induced noncoding RNA modulates expression of Dicer-regulated genes. *Proc. Natl. Acad. Sci. U.S.A.*, **105**, 12897-12902.

54. Zhang, C., Montgomery, T.A., Fischer, S.E., Garcia, S.M., Riedel, C.G., Fahlgren, N., Sullivan, C.M., Carrington, J.C. and Ruvkun, G. (2012) The *Caenorhabditis elegans* RDE-10/RDE-11 complex regulates RNAi by promoting secondary siRNA amplification. *Curr Biol.,* **22**, 881-90.

55. Yang, H., Zhang, Y., Vallandingham, J., Li, H., Floren, L. and Mak, H.Y. (2012) The RDE-10/RDE-11 complex triggers RNAi-induced mRNA degradation by association with target mRNA in *C. elegans*. *Genes Dev.,* **26**, 846-56.

56. Vastenhouw, N.L., Fischer, S.E., Robert, V.J., Thijssen, K.L., Fraser, A.G., Kamath, R.S., Ahringer, J and Plasterk, R.H. (2003) A genome-wide screen identifies 27 genes involved in transposon silencing in *C. elegans*. *Curr Biol.,* **13**, 1311-6.

57. Chen, C.C., Simard, M.J., Tabara, H., Brownell, D.R., McCollough, J.A. and Mello, C.C. (2005) A member of the polymerase beta nucleotidyltransferase superfamily is required for RNA interference in *C. elegans*. *Curr Biol.*, **15**, 378-83.

58. Phillips, C.M., Montgomery, T.A., Breen, P.C. and Ruvkun, G. (2012) MUT-16 promotes formation of perinuclear mutator foci required for RNA silencing in the *C. elegans* germline. *Genes Dev.*, **26**, 1433-44.

59. Uebel, C.J., Anderson, D.C., Mandarino, L.M., Manage, K.I., Aynaszyan, S. and Philips, C.M. (2018) Distinct regions of the intrinsically disordered protein MUT-16 mediate assembly of a small RNA amplification complex and promote phase separation of Mutator foci. *PLoS Genet*, **14**, e1007542.

60. Sarkies, P., Selkirk, M.E., Jones, J.T., Blok, V., Boothby, T., Goldstein, B., Hanelt, B., Ardilia-Garcia, A., Fast, N.M., Schiffer, P.M. *et al.* (2015) Ancient and novel small RNA pathways compensate for the loss of piRNAs in multiple independent nematode lineages. *PLoS Biol.,* **13,** e1002061.

61. Blumenfeld,A. and Jose,A.M. (2016) Reproducible features of small RNAs in *C. elegans* reveal NU RNAs and provide insights into 22G RNAs and 26G RNAs. *RNA*, **22**,184-192.

62. Gent, J.I., Lamm, A.T., Pavelec, D.M., Maniar, J.M., Parameswaran, P., Tao, L., Kennedy, S. and Fire, A.Z. (2010) Distinct phases of siRNA synthesis in an endogenous RNAi pathway in *C. elegans* soma. *Mol Cell.*, **37**, 679-89.

63. Simmer,F., Tijsterman,M., Parrish,S., Koushika,S.P., Nonet,M.L., Fire,A., Ahringer,J. and Plasterk,R.H. (2002) Loss of the putative RNA-directed RNA polymerase RRF-3 makes *C. elegans* hypersensitive to RNAi. *Curr. Biol.*, **12**, 1317-1319.

64. Maniar, J.M. and Fire, A.Z. (2011) EGO-1, a *C. elegans* RdRP, modulates gene expression via production of mRNA-templated short antisense RNAs. *Curr Biol.,* **21**, 449-59.

65. Pak, J., Maniar, J.M, Mello, C.C. and Fire, A. (2012) Protection from feed-forward amplification in an amplified RNAi mechanism. *Cell*, **151**, 885-99.

66. Calixto,A., Chelur,D., Topalidou,I., Chen,X. and Chalfie,M. (2010) Enhanced neuronal RNAi in *C. elegans* using SID-1. *Nat. Methods*, **7**, 554-559.

67. Lee, R.C., Hammel, C.M. and Ambros, V. (2006) Interacting endogenous and exogenous RNAi pathways in *Caenorhabditis elegans*. *RNA*, **12**, 589-97.

68. Aoki, K., Moriguchi, H., Yoshioka, T., Okawa, K. and Tabara, H. (2007) In vitro analyses of the production and activity of secondary small interfering RNAs in *C. elegans*. *EMBO*, **26**, 5007-19.

69. Lewis, S.H., Quarles, K.A., Yang, Y., Tanguy, M., Frézal, L., Smith, S.A., Sharma, P.P., Cordaux, R., Gilbert, C., Giraud, I. *et al.* (2018) Pan-arthropod analysis reveals somatic piRNAs as an ancestral defence against transposable elements. *Nat Ecol Evol*, **2**,174–81.

70. Waldron F.M., Stone G.N. and Obbard D.J. (2018) Metagenomic sequencing suggests a diversity of RNA interference-like responses to viruses across multicellular eukaryotes. *PLoS Genet*, **14**, e1007533.

71. Félix, M.A., Ashe, A., Piffaretti, J., Wu, G., Nuez, I., Bélicard, T., Jiang, Y., Zhao, G., Franz, C.J., Goldstein L.D. *et al.* (2011) Natural and experimental infection of *Caenorhabditis* nematodes by novel viruses related to nodaviruses. *PLoS Biol*, **9**, e1000586.

72. Franz, C.J., Renshaw, H., Frezal, L., Jiang, Y., Félix, M.A. and Wang, D. (2014) Orsay, Santeuil and Le Blanc viruses primarily infect intestinal cells in *Caenorhabditis* nematodes. *Virology*, **5**, 255-64.

73. Buganim, Y., Faddah, D.A., Cheng, A.W., Itskovich, E., Markoulaki, S., Ganz, K., Klemm, S.L., Van Ourdenaarden, A. and Jaenisch, R. (2012) Single-cell expression analyses during cellular reprogramming reveal an early stochastic and late hierarchic phase. *Cell*, **150**, 1209-22.

74. Liberali, P., Snijder, B. and Pelkmans, L. (2014) A hierarchical map of regulatory genetic interactions in membrane trafficking. *Cell*, **157**, 1473-87.

75. Gut, G., Hermann, M.D., Pelkmans, L. (2018) Multiplexed protein maps link subcellular organization to cellular states. *Science*, **361**, eaar7042.

FIGURES AND FIGURE LEGENDS

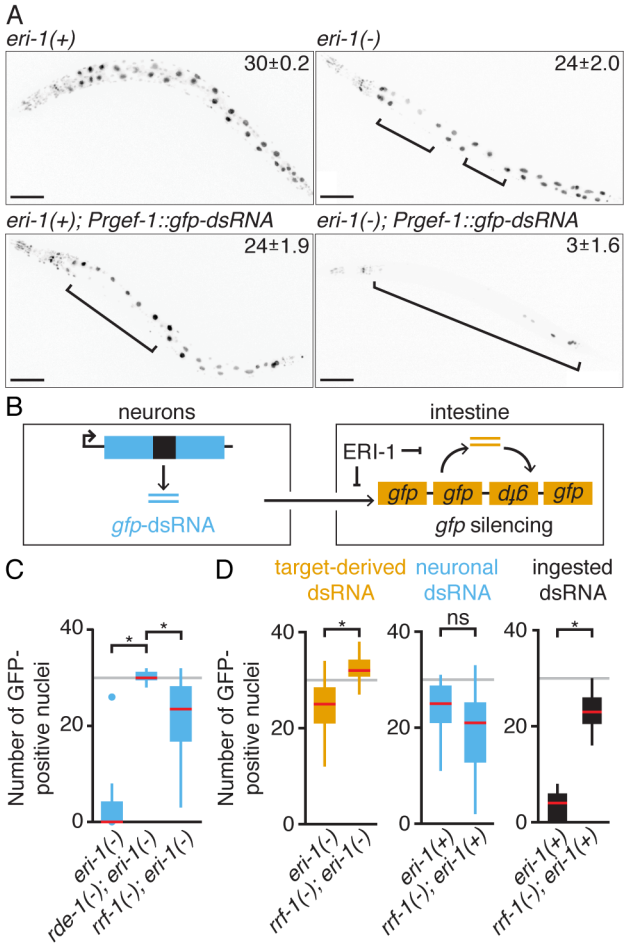

Figure 1: Silencing by different sources of double-stranded RNA show synergy and can have different requirements for the RNA-dependent RNA polymerase RRF-1. (**A**) Silencing upon loss of *eri-1* and by neuronal dsRNA shows synergy. Representative L4-staged animals that express GFP (black) in all tissues (*sur-5::gfp*, top) and animals that in addition express dsRNA against *gfp* in neurons (*Prgef-1::gfp-dsRNA*, *bottom*) in *eri-1(+)* (i.e., wild-type) or *eri-1(-)* backgrounds (left or right, respectively) are shown. Brackets indicate silenced intestinal nuclei. Average numbers of GFP positive intestinal nuclei are indicated with 95% confidence intervals (n = 20 animals). Scale bar = 50 μm. (**B**) Schematic of *gfp* silencing in intestinal cells. Silencing by neuronal dsRNA (cyan) and by dsRNA made from a multicopy *sur-5::gfp* transgene (orange) are both inhibited by the

endonuclease ERI-1. (**C**) Combined silencing by the two sources of dsRNA is strictly dependent on *rde-1* and partially dependent on *rrf-1*. Silencing was measured by counting the number of GFP-positive intestinal nuclei in *eri-1(-), rde-1(-); eri-1(-)*, or *rrf-1(-); eri-1(-)* animals that all express *Prgef-1::gfp-dsRNA*. Grey line indicates average number of intestinal nuclei in animals expressing *sur-5::gfp* in a wild-type background, n ≥ 20 L4-staged animals, red bars indicate medians, and asterisks indicate p-value <0.05 (Student's t-test). Also see Supplementary Figure S1 for additional alleles of *rrf-1*. (**D**) Unlike silencing upon loss of *eri-1* or by ingested dsRNA, silencing by neuronal dsRNA is independent of RRF-1. Silencing was separately measured for the three sources of dsRNA: *left*, target-derived dsRNA upon loss of *eri-1* in *eri-1(-)* or *eri-1(-); rrf-1(-)* animals, *middle*, neuronal dsRNA upon expression of *Prgef-1::gfp-dsRNA* in *eri-1(+)* or *eri-1(+);rrf-1(-)* animals, or *right*, ingested dsRNA from bacteria expressing *gfp-dsRNA* in *eri-1(+)* or *eri-1(+); rrf-1(-)* animals. Red bars, grey line, n, and asterisks are as in C, and ns = not significant.

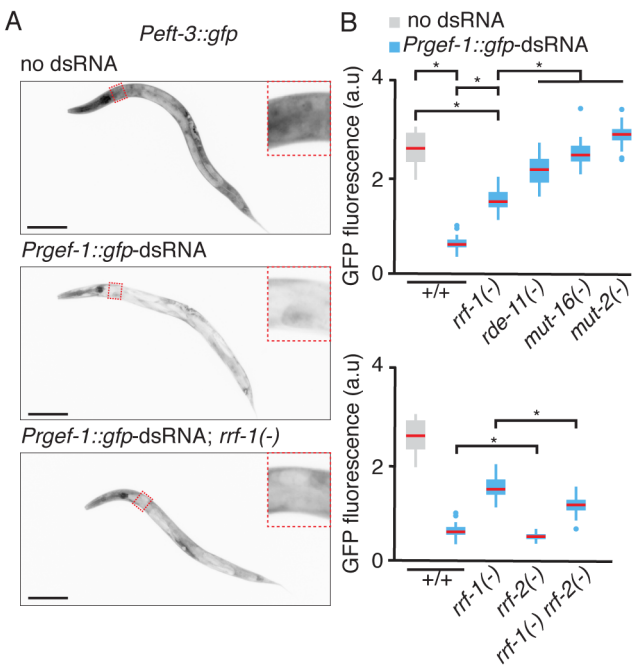

Figure 2: RRF-1-independent silencing by neuronal dsRNA requires some components of the RNAi pathway but does not require RRF-2. (**A**) RRF-1-independent silencing by neuronal dsRNA is detectable for single-copy target sequences. Representative L4-staged animals that express GFP from a single-copy transgene in all tissues (*Peft-3::gfp*, *top*) and animals that in addition express *Prgef-1::gfp*-dsRNA in *rrf-1(+)* or *rrf-1(-)* backgrounds (*middle* or *bottom*, respectively) are shown. Insets are representative of the region quantified in multiple animals in B. Scale bar = 50 μm. Also see Supplementary Figure S3 for additional targets. (**B**) RRF-1-independent silencing of *Peft-3::gfp* requires *rde-11*, *mut-16*, and *mut-2/rde-3* but not *rrf-2*. GFP fluorescence was quantified (using arbitrary units (a.u.) in regions illustrated in A) in control animals that do not express *Prgef-1::gfp*-dsRNA (grey) and in wild-type (+/+), *rrf-1(-)*, *rde-11(-)*, *mut-16(-)*, *mut-2(-), rrf-2(-), or rrf-1(-) rrf-2(-)* animals that express *Prgef-1::gfp*-dsRNA (cyan). Effects of removing known RNAi pathway components (*top*) or a putative RdRP RRF-2 (*bottom*) are separately indicated. Data from top (first 3 bars) are replotted in bottom to facilitate comparison. Red bars indicate medians, asterisks indicate p-value < 0.05 (Two-way

ANOVA for *rrf-2* comparisons and t-test for all other comparisons), and n > 25 L4-staged animals. See Supplementary Figure S4 for details of *rrf-2* deletion.

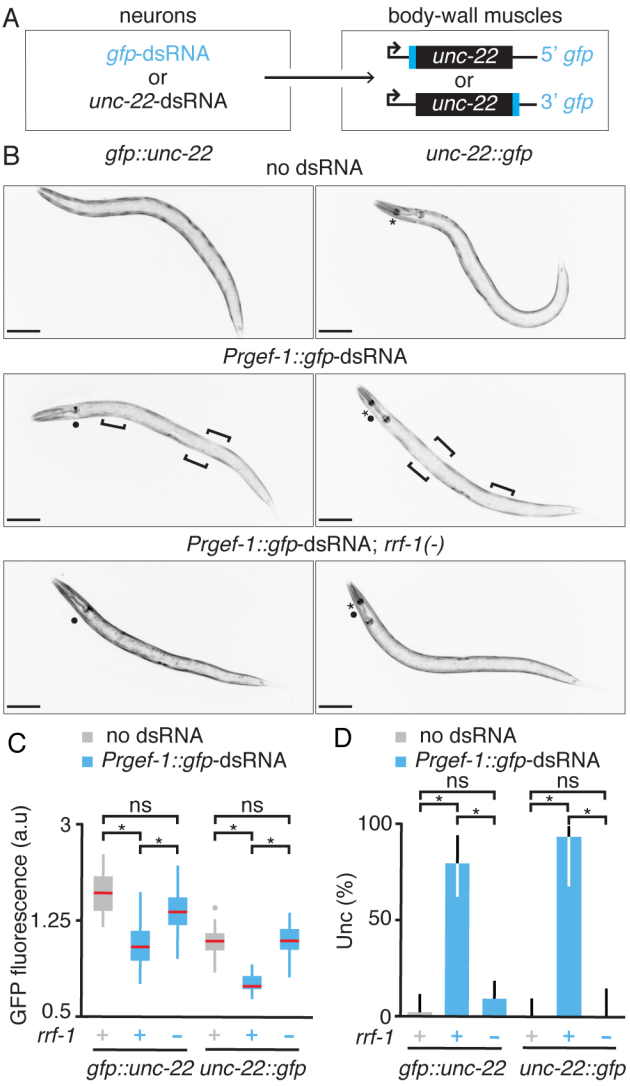

Figure 3: Changing the gene context of a target sequence can change the RRF-1 requirement for silencing that sequence. (**A**) Strategy for combining target sequences from experiments that showed different RRF-1 requirements to test silencing of a single chimeric target by neuronal dsRNA. The *gfp* sequence (cyan) was inserted into the *unc-22* gene (black) at either the 5' or 3' ends to generate single chimeric target genes that can be silenced by either *gfp-dsRNA* or *unc-22-dsRNA*. See Supplementary Figure S4 for details of *gfp* insertions. (**B-D**) Silencing of chimeric targets with *unc-22* and *gfp* sequence by neuronal *gfp-dsRNA* requires RRF-1. (**B**) Representative L4-staged animals that express GFP from chimeric genes (*Punc-22::gfp::unc-22*, left or *Punc-22::unc-22::gfp*,

right) and animals that in addition express *Prgef-1::gfp-dsRNA* in *rrf-1(+)* or *rrf-1(-)* backgrounds (*middle* or *bottom*, respectively) are shown. Fluorescence in the pharynx is observed in some cases because of expression from *Punc-22::unc-22::gfp* (asterisk, see Materials and Methods) and/or fluorescence from *Pmyo-2::DsRed2* (circle, co-injection marker for *Prgef-1::gfp*-dsRNA) detected through the filters for GFP (see Materials and Methods). Scale bar = 50 µm. (**C**) GFP fluorescence from either chimeric gene (*Punc-22::gfp::unc-22* or *Punc-22::unc-22::gfp*) was quantified (posterior to the pharynx) in control animals (*rrf-1(+)*) that do not express *Prgef-1::gfp-dsRNA* (grey) and in animals that express *Prgef-1::gfp-dsRNA* (cyan) in *rrf-1(+)* and *rrf-1(-)* backgrounds. Red bars, a.u., and n are as in 2B, asterisks indicate p-value <0.05 (Student's t-test), and ns = not significant. (**D**) Percentage of animals that showed twitching (%Unc) expected upon silencing of either chimeric transcript (*unc-22::gfp* or *gfp::unc-22*) was scored for all strains analyzed in (C). Error bars indicate 95% confidence interval, asterisks indicate p-value < 0.05 (Student's t-test), ns = not significant, and n=50 L4-staged animals. Also see Supplementary Figure S5 for silencing by *Prgef-1::unc-22*-dsRNA.

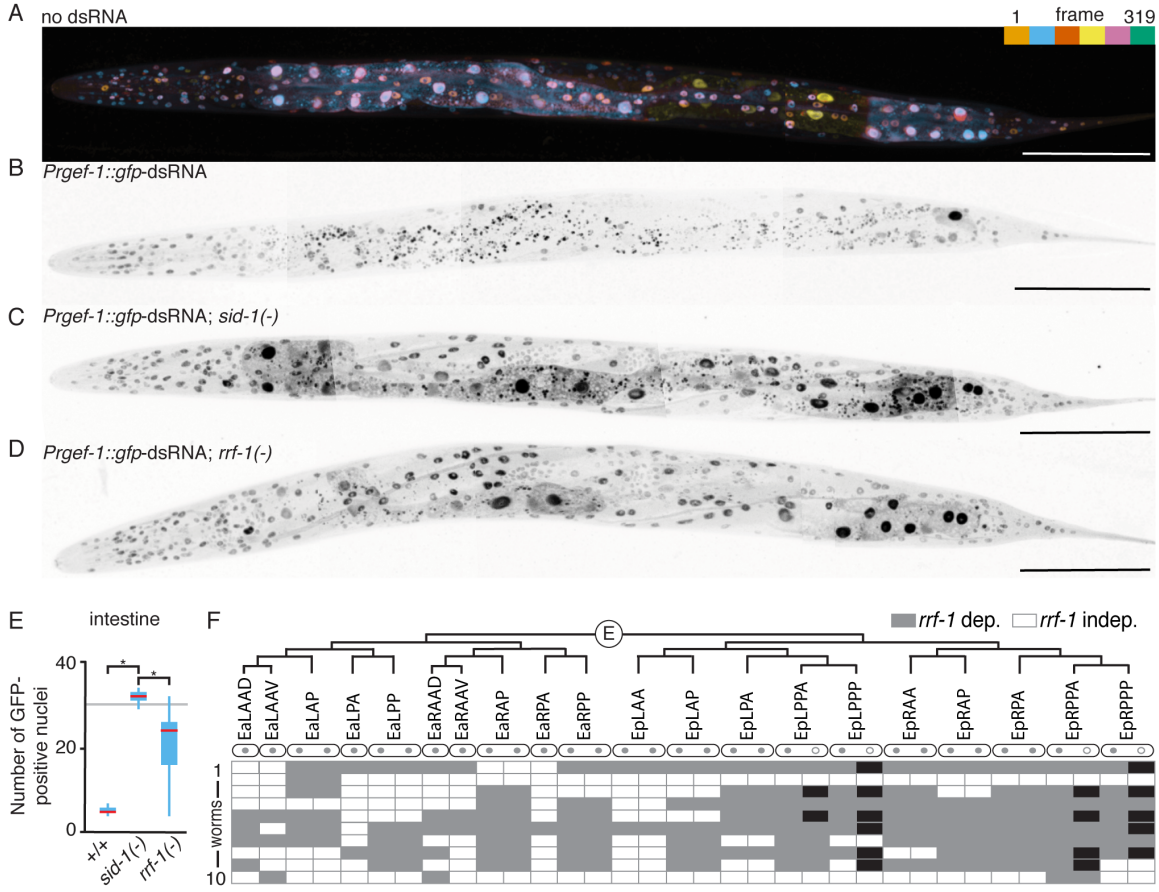

Figure 4: Identities of cells that require RRF-1 for silencing by neuronal dsRNA vary from animal to animal. (**A**) GFP expression from the *sur-5::gfp* chimeric gene enables simultaneous visualization of most somatic nuclei in *C. elegans*. A depth coded (one color for ~53 frames) projection of 5 Z-stacks that were stitched together from a single L4-staged animal is shown (also see Materials and Methods). Scale bar = 100 µm. (**B-D**) Expression of *gfp-dsRNA* in neurons causes silencing throughout the animal that is entirely dependent on SID-1 and partially dependent on RRF-1. Representative images of L4-staged *sur-5::gfp* animals that express *Prgef-1::gfp-dsRNA* (B) and additionally lack *sid-1* (C) or *rrf-1* (D) are shown. Maximum intensity projections were stitched together to generate whole-worm images. Presence of *gfp*-dsRNA causes worms to twist because of the *rol-6* co-injection marker. Scale bar = 100µm. See Supplementary Figure S4 for details of *gfp* insertion. (**E**) RRF-1-independent silencing by neuronal dsRNA is readily detected in

intestinal cells and is highly variable. Numbers of GFP-positive intestinal nuclei (see Materials and Methods for thresholds used) were counted in *sur-5::gfp* animals that express *Prgef-1::gfp-dsRNA* (+/+) and in animals that additionally lack *sid-1* or *rrf-1*. Red bar, grey line, and asterisks are as in Figure 1C and n=10 L4-staged animals. (**F**) Identities of intestinal cells that require RRF-1 for silencing vary from animal to animal. The E blastomere divides to generate 20 intestinal cells (EaLAAD to EpRPPP). Of the 20, 10 undergo nuclear division without cell division (two grey circles per cell), 4 sometimes undergo similar nuclear division (one grey circle and one open circle per cell), and 6 do not undergo any division (one grey circle per cell). GFP-positive and GFP-negative nuclei were scored as *rrf-1*-dependent (grey) and *rrf-1*-independent (white), respectively, in each of 10 *sur-5::gfp; rrf-1(-); Prgef-1::gfp-dsRNA* L4-staged animals. Every binucleate cell had nuclei that were either both RRF-1-dependent or both RRF-1-independent. Black boxes indicate absence of second nucleus because of lack of nuclear division. See Supplementary Figure S6 for images of additional animals.

SUPPLEMENTARY DATA

SUPPLEMENTARY FIGURES

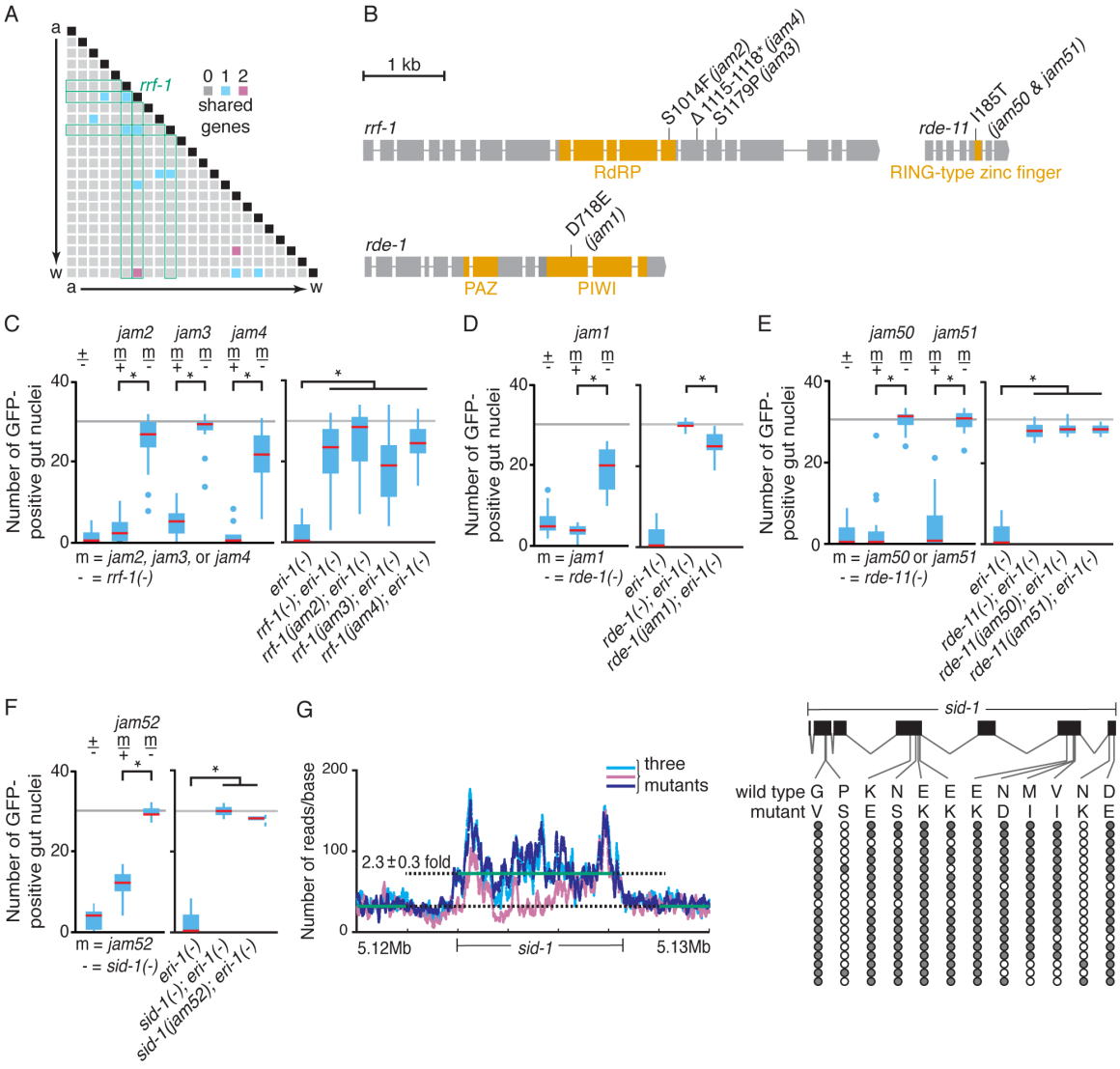

Supplementary Figure S1: Four genes with known roles in RNAi were identified using mutants defective in silencing upon *eri-1* loss and/or by neuronal dsRNA. (**A**) *In silico* comparison of mutations in 23 mutants from a genetic screen identifies 3 alleles of *rrf-1*. Genes mutated in each mutant (a to w) were compared with those mutated in each of the other 22 mutants and the number of genes mutated in pairs of mutants are indicated (0, grey; 1, cyan; or 2, pink). Green outlines indicate three mutants with different mutations in *rrf-1* and black boxes indicate self-comparisons (e.g. a vs a). (**B**) Schematic of *rrf-1*, *rde-*

1 and *rde-11* genes with identified molecular lesions. The gene structures (exons = boxes, introns = lines), identified alleles along with deduced changes in the corresponding proteins (*jam2*(S1014F), *jam3*(S1179P), and *jam4(*Δ1115-1118*, short insertion/deletion resulting in downstream stop codon) in *rrf-1*, *jam1*(D718E) in *rde-1*, and *jam50*(I185T) and *jam51*(I185T) in *rde-11*), and regions encoding known protein domains (RdRP in *rrf-1*, PAZ and PIWI in *rde-1*, and RING-type zinc finger in *rde-11*) are indicated. Scale bar = 1 kb. (**C**) Each isolated allele fails to complement the *rrf-1* null allele and the silencing defect in the three isolated mutants is comparable to that of the null mutant. *Left*, Silencing in test crosses were scored by counting the number of GFP-positive intestinal nuclei in male progeny (m/-) when animals with *jam2*, *jam3* or *jam4* were each crossed to animals with the *rrf-1* null allele (*rrf-1(-)*). Male progeny of mutants crossed with N2 (m/+) and of *rrf-1*(-) crossed to the strain used for mutagenesis (AMJ1, see strain list for complete genotype) (+/-) were scored as controls. *Right*, Silencing was quantified (as in left) in AMJ1 (*eri-1(-)*), in a strain with the *rrf-1* null mutation introgressed into the AMJ1 background (*eri-1(-); rrf-1(-)*), and in strains with each of the three isolated *rrf-1* alleles in the AMJ1 background (*eri-1(-); rrf-1 (jam2, jam3 or jam4)*). Red bar, grey line, n and asterisks are as in Figure 1C. (**D-F**) Complementation testing and comparison of isolated mutants with null mutants of *rde-1*, *rde-11,* and *sid-1.* Tests and comparisons were done as described for *rrf-1* in (C). Unlike in *rde-1* null mutants, silencing is detectable in *rde-1(jam1)* animals (D), indicating that the *jam1* mutation results in a partial loss of function. Both *jam50* and *jam51* mapped to chromosome IV and an examination of all mutations identified by whole genome sequencing of each mutant revealed an identical mutation in *rde-11*. Sequencing of the exons of *sid-1* in animals with *jam52* did not reveal any mutations although *jam52* maps to chromosome V and complements *rde-1* but not *sid-1*. Red bar, grey line, n and asterisk are as in Figure 1C. (**G**) One of the transgenes present in AMJ1 includes a mutated copy of *sid-1* gene sequences incorporated from a PCR fragment. *Left*, Illumina sequencing

reads covering each base for three different mutants (cyan, navy, magenta) indicate that the average coverage (green lines) within the *sid-1* gene is ~2 fold higher than that in surrounding regions, consistent with the presence of an additional copy in the background. *Right*, Twelve changes (in >15% of reads covering a base) that altered the encoded amino acid (wild-type and mutant residues are indicated) were detected in 2 to 19 of 19 sequenced mutants (filled circles). Consistently, this mutated copy of *sid-1*, which is a part of the *qtIs50* transgene, is non-functional (95.3% silencing of *dpy-7* in *qtIs50* animals versus 1.7% silencing in *sid-1(-); qtIs50* animals by feeding RNAi, n>40 L4-staged animals).

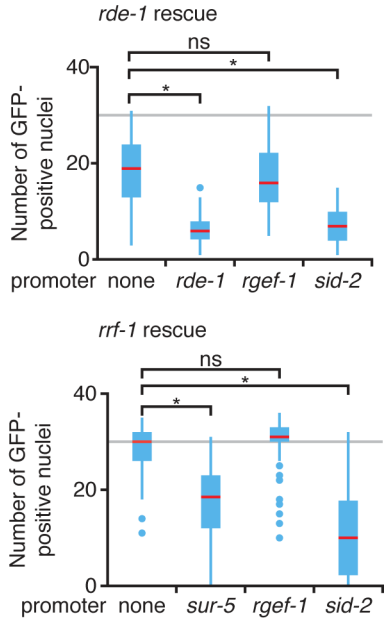

Supplementary Figure S2: *rde-1* and *rrf-1* are required in the intestine for silencing by neuronal dsRNA. *Top*, Rescue of *rde-1(jam1)* using tissue-specific promoters indicates that RDE-1 functions in intestinal cells but not in neurons to enable silencing by neuronal dsRNA. The number of GFP-positive intestinal nuclei in *rde-1(jam1)* animals that were transformed with either a co-injection marker alone (none) or a co-injection marker along with *rde-1(+)* expressed under its own (*rde-1*), intestine-specific (*sid-2*), or neuron-specific (*rgef-1*) promoter were counted. *Bottom*, Rescue of *rrf-1(jam3)* using tissue-specific promoters indicates that RRF-1 functions in intestinal cells but not in neurons to enable silencing by neuronal dsRNA. The number of GFP-positive intestinal nuclei in *rrf-1(jam3)* animals that were transformed with either a co-injection marker alone (none) or a co-injection marker along with *rrf-1(+)* expressed under a somatic (*sur-5*), intestine-specific (*sid-2*), or neuron-specific (*rgef-1*) promoter were counted. Red bar, grey line, n and asterisks are as in Figure 1C, and ns = not significant.

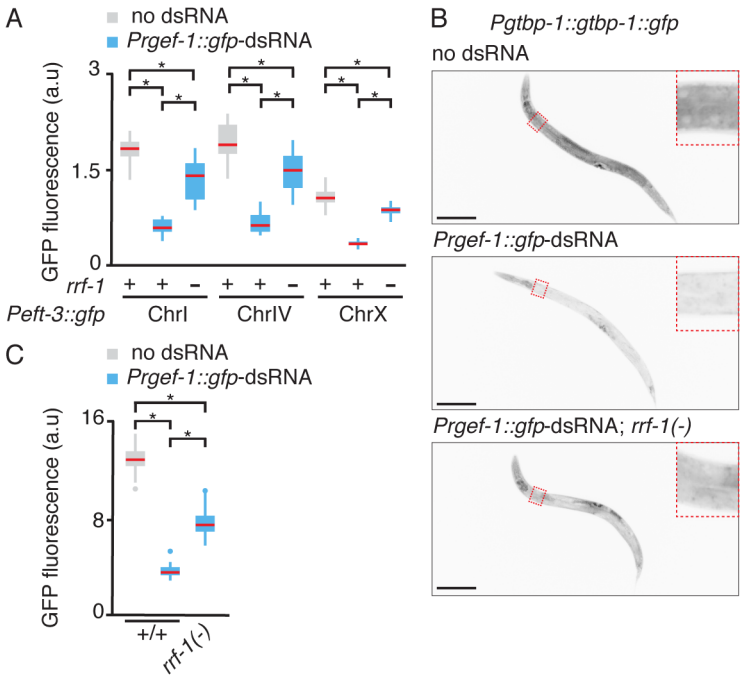

Supplementary Figure S3: RRF-1-independent silencing can occur at multiple *gfp* targets expressed under the control of different regulatory elements. (**A**) RRF-1-independent silencing does not depend on chromosomal location of target sequences. Effect of *Prgef-1::gfp-dsRNA* and loss of *rrf-1* on GFP fluorescence in animals with *Peft-3::gfp* transgenes located on different chromosomes was quantified as in Figure 2B. Grey boxes, cyan boxes, red bars, n, and asterisks are as in Figure 2B. (**B-C**) A single-copy gene fusion generated using Cas9-based genome editing can be silenced by neuronal dsRNA in *rrf-1(-)* animals. Representative L4-staged animals that express GFP in all tissues (*Pgtbp-1::gtbp-1::gfp*, *top*) and animals that in addition express *Prgef-1::gfp-dsRNA* in *rrf-1(+)* or *rrf-1(-)* backgrounds (*middle* or *bottom*, respectively) are shown (B). Insets are representative of the region quantified in multiple animals. Quantification of silencing for GFP expressed from *Pgtbp-1::gtbp-1::gfp* is shown (C). Grey boxes, cyan boxes, red bars, n, and asterisks are as in Figure 2B. Scale bar = 50 µm.

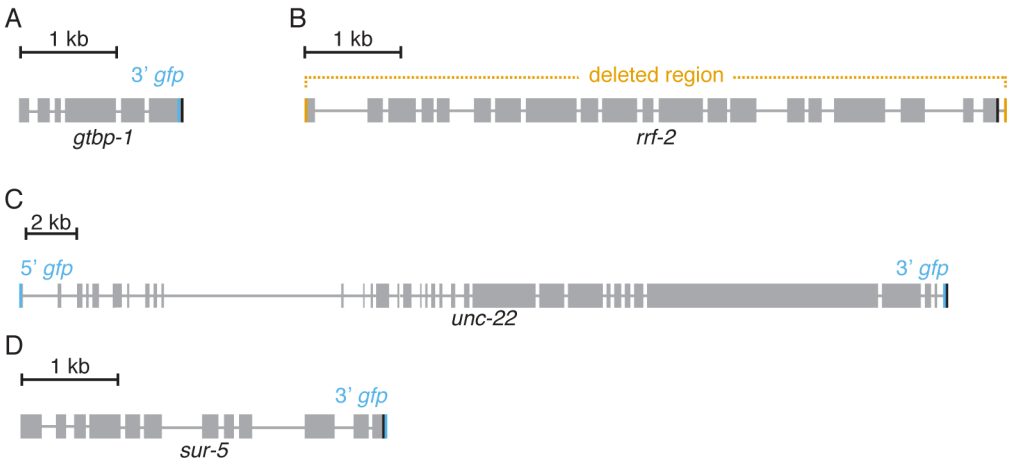

Supplementary Figure S4: Schematic of genomic changes made using Cas9-based genome editing. Genomic changes introduced into *gtbp-1*, *rrf-2*, *unc-22*, and *sur-5* loci in this study are indicated. The sgRNA target site is indicated (blue for insertions and orange for deletion) on the gene structure (exons = grey boxes, introns = grey lines, stop codon = black). Homology-directed repair templates were used to either insert *gfp* sequences (**A**, **C**, and **D**) or to delete the region between two target sites (**B**). Scale bars are as indicated.

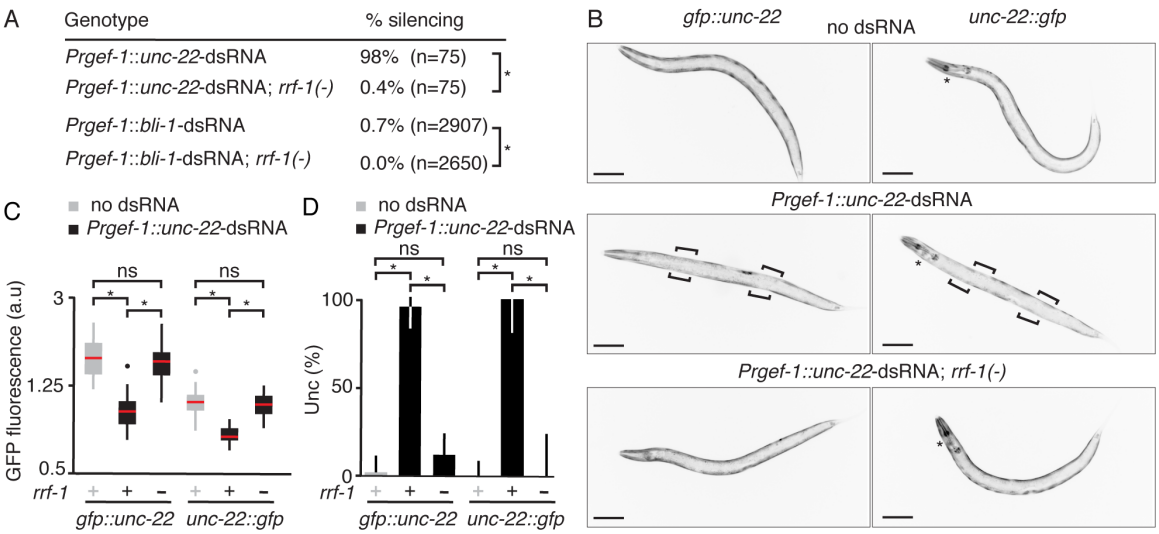

Supplementary Figure S5: A source of neuronal dsRNA that requires RRF-1 for silencing retains the requirement when used to silence chimeric sequences. (**A**) Silencing of *unc-22* or *bli-1* by neuronal dsRNA requires RRF-1. Percentage of animals showing silencing of *unc-22* or *bli-1* by matching dsRNA expressed under a neuronal promoter (*Prgef-1*) was measured in *rrf-1(+)* or *rrf-1(-)* backgrounds. The number of gravid-adult (for *bli-1*) or L4-staged (for *unc-22*) animals scored are indicated in brackets and asterisks indicate p-value < 0.05 (Wilson's estimates for proportions). (**B-D**) Effect of *rrf-1* loss on silencing of chimeric targets with *unc-22* and *gfp* sequence by *Prgef-1::unc-22-dsRNA* was characterized as in Figure 3 for *Prgef-1::gfp-dsRNA*. Note that *Prgef-1::DsRed2* was used as a co-injection marker for *Prgef-1::unc-22-dsRNA* and therefore the pharyngeal expression from the *Pmyo-2::DsRed2* co-injection marker used in Figure 3 is not seen here.

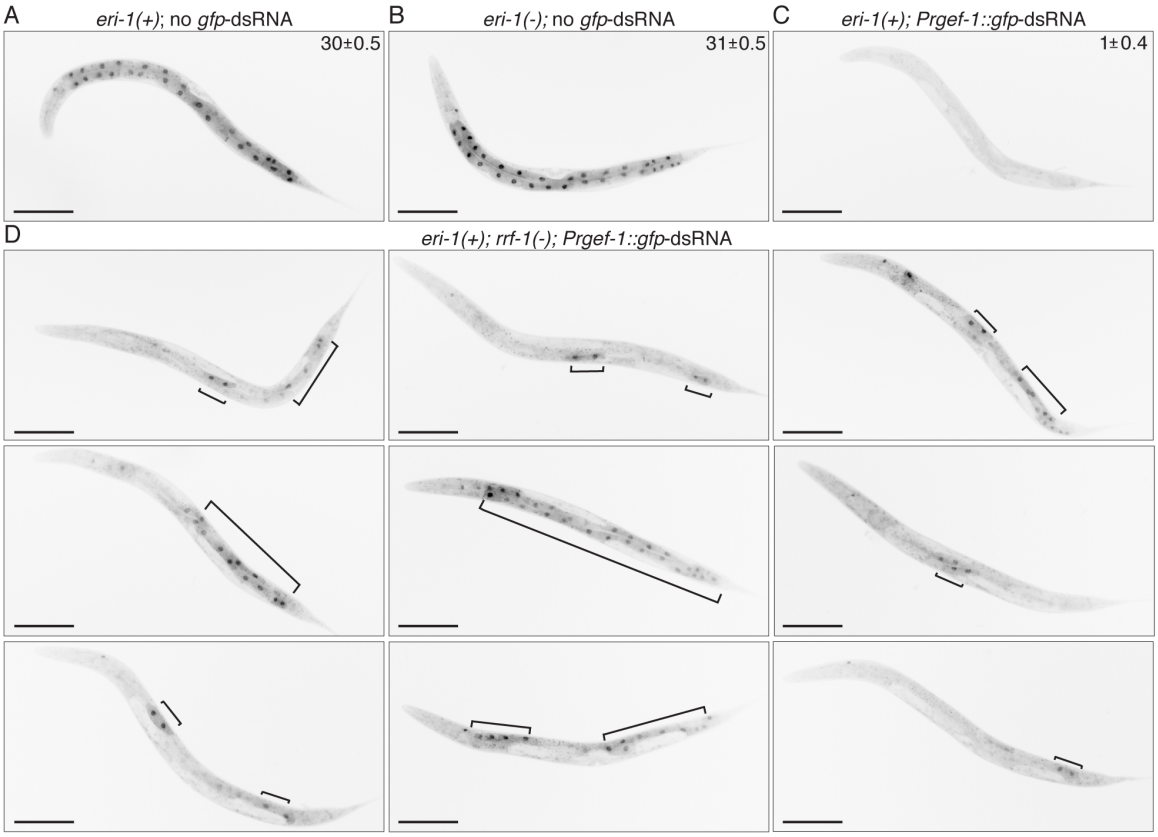

Supplementary Figure S6: Single-copy *sur-5::gfp* is not subject to self-silencing upon *eri-1* loss but can be robustly silenced by neuronal dsRNA, revealing different patterns of RRF-1-independent silencing. (**A-C**) Representative *sur-5::gfp* animals in an *eri-1(+)* (i.e., wild-type) background (A) or an *eri-1(-)* background (B) that do not express *gfp*-dsRNA or in an *eri-1(+)* background (C) that expresses *Prgef-1::gfp-dsRNA* are shown. (**D**) A collection of L4-staged *sur-5::gfp* animals that express *Prgef-1::gfp-dsRNA* in an *eri-1(+); rrf-1(-)* background is shown. Brackets indicate intestinal nuclei that appear to require RRF-1 for complete silencing. Average numbers of GFP-positive intestinal nuclei are indicated in A-C, errors indicate 95% confidence intervals, and n = 25 L4-staged animals. Scale bar = 50 μm.

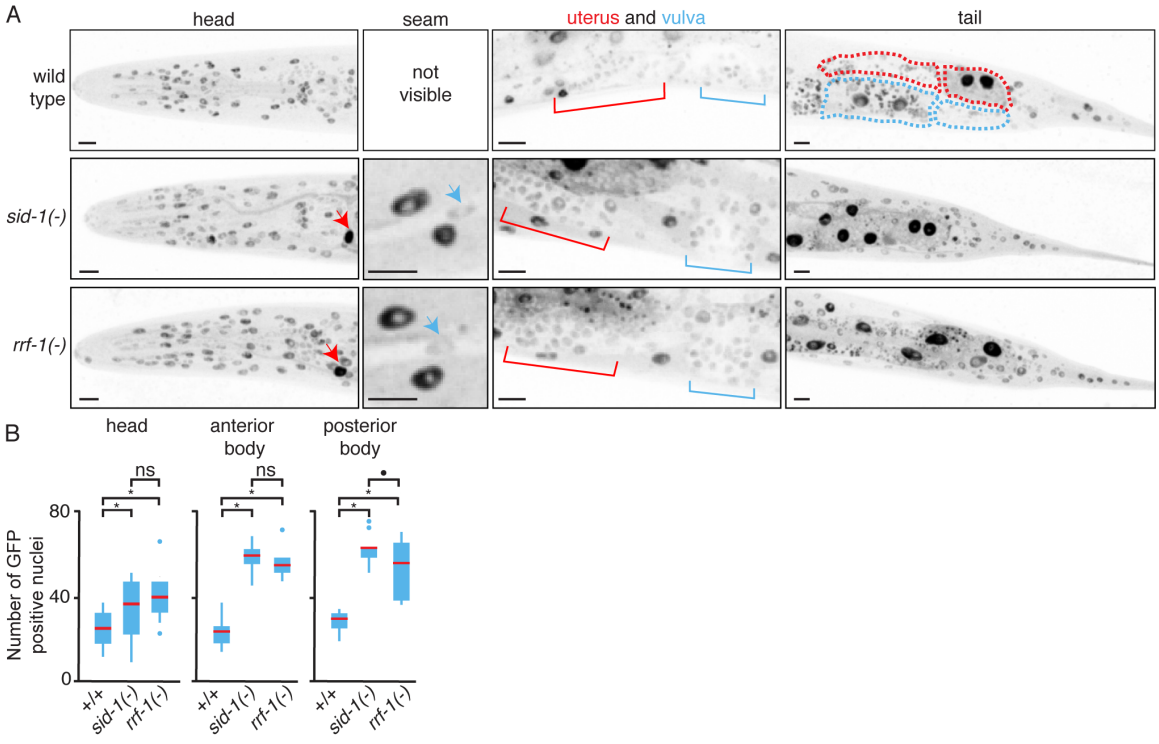

Supplementary Figure S7: A single-cell resolution view of silencing by neuronal dsRNA reveals differences among cell types and a requirement for RRF-1 in most non-intestinal cells. Silencing of individual nuclei was examined using confocal microscopy of *sur-5::gfp* animals that express *Prgef-1::gfp*-dsRNA in a wild-type, *sid-1(-),* or *rrf-1(-)* background. (**A**) Representative images showing maximum intensity projections that highlight extents of silencing in different cell types. The excretory canal cell (red arrow), seam cell (cyan arrow), cells of the developing uterus (red bracket), cells of the developing vulva (cyan bracket), and intestinal cells near the tail of wild-type animals (cyan or red dashed lines for each pair of sister cells) are indicated. Scale bar = 10μm. Seam cells were silenced and not visible in wild-type animals. (**B**) Quantification of silencing in non-intestinal cells. Numbers of GFP-positive nuclei (see Materials and Methods for thresholds used) were counted in the head (anterior to the posterior bulb of the pharynx), anterior body (anterior to the vulva), and posterior body (posterior to the vulva). Counts included most body-wall muscle and hypodermal cells throughout the animal but specifically excluded some other

cell types. The excretory canal cell (detected in 0/10 *sur-5::gfp*, 10/10 *sid-1(-); sur-5::gfp* and 10/10 *rrf-1(-); sur-5::gfp* animals) and intestinal cells (separately presented in Figure 4E) were excluded from this analysis based on their large sizes and positions. Cells of the developing uterus and vulva, which remained visible in all tested strains, were excluded based on their small sizes and collective morphology. Seam cells, which show faint expression were excluded because they could not be reliably detected in most Z-slices that were away from the coverslip. Red bars indicate medians, asterisks and circle indicate p-value < 0.05 and p-value = 0.08, respectively (Student's t-test), and n = 10 L4-staged animals.

SUPPLEMENTARY MATERIALS AND METHODS

Table S1. Strains Used.

Strains	Genotype
N2	Wild type
AMJ1	*qtIs50 [Pmyo-3::DsRed2, Pmyo-3::DsRed2-dsRNA & sid-1(+)] II; juIs73 [Punc-25::gfp] qtIs49 [Prgef-1::gfp-dsRNA & pRF4] III; eri-1(mg366) nrIs20 [sur-5::gfp] IV*
AMJ2	*qtIs49 III; eri-1(mg366) nrIs20 IV; sid-1(qt9) V*
AMJ38	*rrf-1(ok589) I; qtEx136 [Prgef-1::unc-22-dsRNA]*
AMJ86	*rrf-1(jam2) I; qtIs50 II; juIs73 qtIs49 III; eri-1(mg366) nrIs20 IV*
AMJ87	*rrf-1(jam3) I; qtIs50 II; juIs73 qtIs49 III; eri-1(mg366) nrIs20 IV*
AMJ109	*rrf-1(jam4) I; qtIs50 II; juIs73 qtIs49 III; eri-1(mg366) nrIs20 IV*
AMJ113	*qtIs50 II; juIs73 qtIs49 III; eri-1(mg366) nrIs20 IV; rde-1(jam1) V*
AMJ116	*qtIs50 II; juIs73 qtIs49 III; eri-1(mg366) nrIs20 IV; rde-11(jam51) V*
AMJ119	*qtIs50 II; juIs73 qtIs49 III; eri-1(mg366) nrIs20 IV; rde-11(jam50) V*
AMJ120	*qtIs50 II; juIs73 qtIs49 III; eri-1(mg366) nrIs20 IV; sid-1(jam52) V*
AMJ233	*qtIs50 II; juIs73 qtIs49 III; eri-1(mg366) nrIs20 IV; rde-1(jam1) V [1X*
AMJ241	*rrf-1(jam3) I; qtIs50 II; juIs73 qtIs49 III; eri-1(mg366) nrIs20 IV [1X*
AMJ245	*rrf-1(ok589) I; qtIs49 III; eri-1(mg366) nrIs20 IV*
AMJ246	*rrf-1(ok589) I; nrIs20 eri-1(mg366) IV*
AMJ247	*rrf-1(ok589) I; qtIs49 III; nrIs20 IV*
AMJ294	*rrf-1(jam3) I; qtIs49 III; eri-1(mg366) nrIs20 IV; jamEx71 [Psur-5::rrf-1(+)]*
AMJ295	*rrf-1(jam3) I; qtIs49 III; eri-1(mg366) nrIs20 IV; jamEx72 [Prgef-1::rrf-1(+)]*
AMJ296	*rrf-1(jam3) I; qtIs49 III; eri-1(mg366) nrIs20 IV; jamEx73 [Psid-2::rrf-1(+)]*
AMJ300	*qtIs49 III; nrIs20 IV*
AMJ318	*qtIs49 III; eri-1(mg366) nrIs20 IV; rde-1(ne219) V*
AMJ349	*qtIs49 III; oxSi221 [Peft-3::gfp] II; unc-119(ed3)? III*
AMJ477	*qtEx136*
AMJ793	*jamEx203 [Prgef-1::bli-1dsRNA]*
AMJ964	*rrf-1(ok589) I; jamEx203*
AMJ965	*unc-22(jam77[gfp::unc-22]) IV; qtEx136*
AMJ966	*rrf-1(ok589) I; unc-22(jam77[gfp::unc-22]) IV; qtEx136*
AMJ967	*unc-22(jam77[gfp::unc-22]) IV; qtEx140 [Prgef-1::gfp-dsRNA]*
AMJ968	*rrf-1(ok589) I; unc-22(jam77[gfp::unc-22]) IV; qtEx140*
AMJ969	*unc-22(jam78[unc-22::gfp]) IV; qtEx136*
AMJ970	*rrf-1(ok589) I; unc-22(jam78[unc-22::gfp]) IV; qtEx136*
AMJ971	*unc-22(jam78[unc-22::gfp]) IV; jamEx140*
AMJ972	*rrf-1(ok589) I; unc-22(jam78[unc-22::gfp]) IV; jamEx140*
AMJ973	*rrf-1(ok589) I; oxSi221 II; qtIs49 unc-119(ed3)? III*
AMJ975	*sur-5(jam79 [sur-5::gfp]) IV*

AMJ976	*qtIs49 III; sur-5(jam79 [sur-5::gfp]) IV*
AMJ977	*rrf-1(ok589) I; qtIs49 III; sur-5(jam79 [sur-5::gfp]) IV*
AMJ978	*qtIs49 III; sur-5(jam79 [sur-5::gfp]) IV; sid-1(qt9) V*
AMJ979	*rrf-2(jam36 [deletion]) I; oxSi221 II; qtIs49 unc-119(ed3)? III*
AMJ980	*rrf-1(ok589) rrf-2(jam36 [deletion]) I; oxSi221 II; qtIs49 unc-119(ed3)? III*
AMJ982	*eri-1(mg366) sur-5(jam79) IV*
AMJ986	*qtIs49 unc-119(ed3)? III; oxSi346 [Peft-3::gfp] IV*
AMJ987	*rrf-1(ok589) I; qtIs49 unc-119(ed3)? III; oxSi346 IV*
AMJ988	*qtIs49 unc-119(ed3)? III; oxSi230 [Peft-3::gfp] X*
AMJ989	*rrf-1(ok589) I; qtIs49 unc-119(ed3)? III; oxSi230 X*
AMJ990	*oxSi257 [Peft-3::gfp] I; qtIs49 unc-119(ed3)? III.*
AMJ991	*rrf-1(ok589) I; oxSi257 I; qtIs49 unc-119(ed3)? III.*
AMJ1000	*unc-22(jam77[gfp::unc-22]) IV*
AMJ1001	*unc-22(jam78[unc-22::gfp]) IV*
AMJ1163	*oxSi221 II; qtIs49 unc-119(ed3)? III; rde-11(hj37) IV*
AMJ1177	*mut-2(jam9) I; oxSi221 II; qtIs49 unc-119(ed3)? III*
AMJ1179	*mut-16(pk710) I; oxSi221 II; qtIs49 unc-119(ed3)? III*
AMJ1180	*qtIs49 III; gtbp-1 (ax2053[gtbp-1::gfp])IV*
AMJ1181	*rrf-1(ok589) I; qtIs49 III; gtbp-1 (ax2053[gtbp-1::gfp])IV*
AMJ1183	*qtIs49 III; gtbp-1 (jam83 [gtbp-1::gfp])IV*
AMJ1184	*rrf-1(ok589) I; qtIs49 III; gtbp-1 (jam83[gtbp-1::gfp])IV*
EG6070	*oxSi221 II; unc-119(ed3) III.*
EG6109	*unc-119(ed3) III; oxSi230 X.*
EG6171	*oxSi257 I; unc-119(ed3) III.*
EG6401	*unc-119(ed3) III; oxSi346 IV*
HC196	*sid-1(qt9) V*
HC567	*eri-1(mg366) nrIs20 IV*
HC780	*rrf-1(ok589) I [2x]*
JH3197	*gtbp-1 (ax2053[gtbp-1::gfp])IV*
VS27	*rde-11(hj37) IV*
WM27	*rde-1(ne219) V*

Transgenesis and genome editing:

To express *rde-1(+)* under its own promoter (*Prde-1::rde-1(+)*): The *rde-1* promoter, coding sequence, and 3' UTR were amplified from N2 gDNA using the primers P17 and P18. AMJ233 animals were transformed with 10ng/µl of *Prde-1::rde-1(+)* and 40ng/µl of pHC448 in dH_2O to generate three independent transgenic lines.

To express *rde-1(+)* in the neurons (*Prgef-1::rde-1(+)*): The *rgef-1* promoter (*Prgef-1*) was amplified using the primers P19 and P20, and *rde-1(+)* coding sequence and 3' UTR was amplified from N2 gDNA using the primers P21 and P22. The two PCR products were used as template and the *Prgef-1::rde-1(+)* fusion product was generated using the primers P23 and P24. AMJ233 animals were transformed with 10ng/µl of *Prgef-1::rde-1(+)* and 40ng/µl of pHC448 in dH_2O to generate three independent transgenic lines.

To express *rde-1(+)* in the intestine (*Psid-2::rde-1(+)*): The *sid-2* promoter (*Psid-2*) was amplified from N2 gDNA using the primers P25 and P26, and *rde-1(+)* coding sequence and 3' UTR was amplified from N2 gDNA using the primers P27 and P22. The two PCR products were used as template and the *Psid-2::rde-1(+)* fusion product was generated using the primers P28 and P24. AMJ233 animals were transformed with 10ng/ul of *Psid-2::rde-1(+)* and 40ng/µl of pHC448 in dH_2O to generate three independent transgenic lines.

To express *rrf-1* in most somatic cells (*Psur-5::rrf-1(+)*): The precise promoter elements that drive *rrf-1* expression are unclear because *rrf-1* is the downstream gene in an operon that includes another RNA-dependent RNA polymerase gene *ego-1*. Therefore, we used the promoter of a somatically expressed gene *sur-5* to express *rrf-1* in most somatic cells. The *sur-5* promoter was amplified from N2 gDNA using the primers P29 and P30. The *rrf-1* gene and its 3'UTR were amplified together from N2 gDNA using the primers P31 and P32. The two PCR products were used as templates to generate the fusion product using the primers P33 and P34. A 1:4 mixture of *Psur-5::rrf-1(+)* (10ng/µl) and pHC448 (40ng/µl)

in 10mM Tris HCl (pH 8.5) was injected into AMJ241 to generate AMJ294 and two other independent transgenic lines.

To express *rrf-1* in intestinal cells (*Psid-2::rrf-1(+)*): The *sid-2* promoter was amplified from N2 gDNA using the primers P35 and P36, and *rrf-1* was amplified along with its 3' UTR using the primers P31 and P32. The two PCR products were used as templates to generate the fusion product using the primers P35 and P34. A 1:4 mixture of *Psid-2::rrf-1(+)* (10ng/µl) and pHC448 (40ng/µl) in 10mM Tris HCl (pH 8.5) was injected into AMJ241 to generate AMJ296 and two other independent transgenic lines.

To express *rrf-1* in the neurons (*Prgef-1::rrf-1(+)*): The *rgef-1* promoter was amplified from N2 gDNA using the primers P37 and P38 and *rrf-1* and its 3'UTR were amplified together using the primers P31 and P32. The two PCR products were used as templates to generate the fusion product using the primers P37 and P34. A 1:4 mixture of *Prgef-1::rrf-1(+)* (10ng/µl) and pHC448 (40ng/µl) in 10mM Tris HCl (pH 8.5) was injected into AMJ241 to generate AMJ295 and two other independent transgenic lines.

To delete *rrf-2* using genome editing: The forward primers P39 and P40 were used to amplify two guide RNAs for the *rrf-2* deletion (Supplementary Figure S4) and the forward primer P41 was used to amplify the guide RNA for the co-conversion marker *dpy-10*. The homology repair templates for *rrf-2* and *dpy-10* were single-stranded DNA oligos (P42 for *rrf-2* and P43 for *dpy-10*). AMJ349 (*Peft-3::gfp; qtIs49*) animals were injected with 5.1 pmol/µl of *rrf-2* guide RNA1, 6.2 pmol/µl of *rrf-2* guide RNA2, 2.3 pmol/µl of *dpy-10* guide RNA, 9.4 pmol/µl of *rrf-2* homology repair template, 6.1 pmol/µl of *dpy-10* homology repair template and 1.5 pmol/µl of Cas9 protein. The deletion was genotyped using 3 primers (P44-P46).

To tag *gtbp-1*, *unc-22* and *sur-5* with *gfp* using genome editing: A single guide RNA was selected <6 base pairs away from the insertion site (Supplementary Figure S4), and *gfp* sequences for the homology template was amplified from pTK2 (a derivative of pPD95.75

– Addgene plasmid #1494, a gift from Andrew Fire) using primers with 35-40 base pair overhangs matching either side of the cut site. Guide RNAs were amplified using the forward primers P47 for *gtbp-1::gfp*, P48 for *gfp::unc-22*, P49 for *unc-22::gfp* and P50 for *sur-5::gfp*. Homology templates were amplified using P51 and P52 for *gtbp-1::gfp*, P53 and P54 for *gfp::unc-22*, P55 and P56 for *unc-22::gfp*, and P57 and P58 for *sur-5::gfp*. N2 animals were injected with 9 to 15 pmol/µl of guide RNA, 0.4 to 0.9 pmol/µl of homology repair template and 1.5 pmol/µl of Cas9 protein. Edited F1 or F2 animals were selected by picking animals that showed GFP fluorescence under the Olympus MVX10 fluorescent microscope. The GFP insertion was genotyped using 3 primers (P59 within GFP along with P60 and P61 for *gfp::unc-22*, or P62 and P63 for *unc-22::gfp,* or P64 and P65 for *sur-5:;gfp*).

Table S2. Oligonucleotides used.

Name	Sequence
P01	cagacctcacgatatgtggaaa
P02	ggaacatatggggcattcg
P03	catttgtgcatttccttcca
P04	atgcttgtgaaatccgggta
P05	ttctggatactcctcggatg
P06	ttatttcgagtcgttcagagc
P07	cggacagaggaagaaatgc
P08	cactattcacaagcattggc
P09	gatttcggactccctatgtg
P10	agttaatgtagcacccgactc
P11	tgccatcgcagatagtcc
P12	tggaagcagctaggaacag
P13	ccgtgacaacagacattcaatc
P14	agtaacagtttcaaatggccg
P15	tcttcactgtacaatgtgacg
P16	aaaagcaccgactcggt
P17	cggagtgagtaccaatgagc
P18	gggacgaagtattgcggag
P19	tttccgatacccccttatatc
P20	aaaattcgaggacatgtcgtcgatgccgtcttc
P21	gaagacggcatcgacgacatgtcctcgaattttcccg
P22	ccggagtgagtaccaatgag
P23	gataccccttatatcagcac
P24	gagcgatgtcatcttgtgacc
P25	ctcattttcgggttcagtgg
P26	aaaattcgaggacatttcctgaaaatatcagggttttg
P27	caaaaccctgatattttcaggaaatgtcctcgaattttcccg
P28	gttcagtggtttgtcaactc
P29	agtatcggaattgagatggg
P30	ccatgacttcgttccgacattctgaaaacaaaatgtaaagttc
P31	atgtcggaacgaagtcatgg

P32	agacacactcttcagcgaac
P33	gaaattgaagacgcaacaaaaac
P34	cgaaaagagaacggagtgtc
P35	ctcattttcgggttcagtgg
P36	ccatgacttcgttccgacatttcctgaaaatatcagggttttg
P37	cgataatctcgtgacactcg
P38	ccatgacttcgttccgacatcgtcgtcgtcgtcgatgc
P39	atttaggtgacactatagcaggcctttcgttatgtcggttttagagctagaaatagcaag
P40	atttaggtgacactatagtctggaaattgcactctgggttttagagctagaaatagcaag
P41	atttaggtgacactatagctaccataggcaccacgaggttttagagctagaaatagcaag
P42	ggtgaaattacttctcgttttgcaggcctttcgtttggtgggctacgttttgatagtcatgtcacgaaat
P43	cacttgaacttcaatacggcaagatgagaatgactggaaaccgtaccgcatgcggtgcctatggtagcggagcttca catggcttcagaccaacagccta
P44	ttagcgtctcttagctgtctg
P45	ctaaacttacaagcccatagg
P46	cgcaattctcgtagatcaaac
P47	atttaggtgacactatagcacgaggtggtatgcgcaggttttagagctagaaatagcaag
P48	atttaggtgacactatagaagcgcggtgcgccaaccagttttagagctagaaatagcaag
P49	atttaggtgacactataggtggcaggatgattagacagttttagagctagaaatagcaag
P50	atttaggtgacactatagatctttaattttatttcaagttttagagctagaaatagcaag
P51	ggttcgggtggtgctccacgaggtggtatgcgcatgagtaaaggagaagaacttttc
P52	cttctaattttgtcccgcattttggaaaccgcttttgtatagttcatccatgcc
P53	attaaaagtcgtgcgccggcccctccaacttcgaccatgagtaaaggagaagaacttttc
P54	aatggacggtttctgggtgaagcgcggtgcgccaaccattttgtatagttcatccatgcc
P55	gcaattgcaaaatatgcggcagctcttctccttgtcatgagtaaaggagaagaacttttc
P56	aaatataatgaagtttaaagtggtggtggcaggatgactatttgtatagttcatccatgc
P57	ccagaatctcttgatcatttcgttcaatacagacttatgagtaaaggagaagaacttttc
P58	gaaggaaagcgtgaatatataattttcagaaacagaaacaaataaatcgttgaaataaaattaaagactatttgtata gttcatccatgc
P59	gtgtccaagaatgtttccatc
P60	cgtcatagaagagacagtttg
P61	gaacagagataggtgagatatg
P62	gaatagttgtggatacgctag
P63	ccgggcttattacttgattg

P64	cagccattgtttctaaactcc
P65	aacaggttcaggcaatgagc